



Measurement of Υ production in pp collisions at $\sqrt{s} = 13$ TeV

R. Aaij, Bernardo Adeva, Marco Adinolfi, Ziad Ajaltouni, Simon Akar, Johannes Albrecht, Federico Alessio, Michael Alexander, Alejandro Alfonso Albero, Suvayu Ali, et al.

► To cite this version:

R. Aaij, Bernardo Adeva, Marco Adinolfi, Ziad Ajaltouni, Simon Akar, et al.. Measurement of Υ production in pp collisions at $\sqrt{s} = 13$ TeV. *Journal of High Energy Physics*, 2018, 2018 (7), pp.134. 10.1007/JHEP07(2018)134 . hal-01796872

HAL Id: hal-01796872

<https://hal.science/hal-01796872>

Submitted on 18 Jul 2023

HAL is a multi-disciplinary open access archive for the deposit and dissemination of scientific research documents, whether they are published or not. The documents may come from teaching and research institutions in France or abroad, or from public or private research centers.

L'archive ouverte pluridisciplinaire **HAL**, est destinée au dépôt et à la diffusion de documents scientifiques de niveau recherche, publiés ou non, émanant des établissements d'enseignement et de recherche français ou étrangers, des laboratoires publics ou privés.



CERN-EP-2018-054
 LHCb-PAPER-2018-002
 1 August 2018

Measurement of Υ production in pp collisions at $\sqrt{s} = 13$ TeV

LHCb collaboration[†]

Abstract

The production cross-sections of $\Upsilon(1S)$, $\Upsilon(2S)$ and $\Upsilon(3S)$ mesons in proton-proton collisions at $\sqrt{s} = 13$ TeV are measured with a data sample corresponding to an integrated luminosity of $277 \pm 11 \text{ pb}^{-1}$ recorded by the LHCb experiment in 2015. The Υ mesons are reconstructed in the decay mode $\Upsilon \rightarrow \mu^+ \mu^-$. The differential production cross-sections times the dimuon branching fractions are measured as a function of the Υ transverse momentum, p_T , and rapidity, y , over the range $0 < p_T < 30 \text{ GeV}/c$ and $2.0 < y < 4.5$. The ratios of the cross-sections with respect to the LHCb measurement at $\sqrt{s} = 8$ TeV are also determined. The measurements are compared with theoretical predictions based on NRQCD.

Published in JHEP 07(2018)134

© 2018 CERN for the benefit of the LHCb collaboration. CC-BY-4.0 licence.

[†]Authors are listed at the end of this paper.

1 Introduction

The study of heavy quarkonium ($c\bar{c}$ and $b\bar{b}$) production in high-energy hadron collisions provides important information to better understand quantum chromodynamics (QCD). Thanks to theoretical and experimental efforts in the past forty years, the comprehension of hadronic production of heavy quarkonia has been improved significantly. The production of heavy quarkonium in proton-proton (pp) collisions at the Large Hadron Collider (LHC) is expected to start with the production of a heavy quark pair, $Q\bar{Q}$, followed by its hadronization into a bound state. The heavy quark pair $Q\bar{Q}$ is produced mainly via Leading Order (LO) gluon-gluon interactions. Several models have been proposed to describe the underlying dynamics, such as the colour-singlet model (CSM) [1–7] and non-relativistic QCD (NRQCD) [8–10]. In the CSM the intermediate $Q\bar{Q}$ state is supposed to be colourless and has the same quantum numbers as the quarkonium final state, while in NRQCD the calculations also include the colour-octet contribution. However, at present no model can describe both the heavy quarkonium production cross-section and polarisation simultaneously.

The production of $\Upsilon(1S)$, $\Upsilon(2S)$ and $\Upsilon(3S)$ mesons has been studied at LHC by ATLAS [11, 12] and CMS [13, 14] collaborations at centre-of-mass energies of 7 TeV and 13 TeV. The measurements have also been performed by LHCb at centre-of-mass energies of 2.76 TeV [15], 7 TeV [16–19] and 8 TeV [17–20]. The NRQCD calculations can describe the trends of the differential production cross-sections in data for all three Υ states within uncertainties. The measured production cross-section ratios between 7 TeV and 8 TeV [18] as a function of transverse momentum, p_T , are consistently higher than the next-to-leading order NRQCD theory predictions [21], and the ratios as a function of rapidity show a different trend than the predictions [22, 23]. The measurement performed at 13 TeV presented here provides valuable input to study the quarkonium production at a higher centre-of-mass energy, enabling ratios to be determined with respect to data taken at a lower centre-of-mass energy. Most of the theoretical and experimental uncertainties cancel in the ratios, and more stringent constraints on the theoretical models can be obtained.

This paper presents a measurement of the differential production cross-sections times dimuon branching fractions of $\Upsilon(1S)$, $\Upsilon(2S)$ and $\Upsilon(3S)$ mesons, as functions of p_T , and rapidity, y , over the range $0 < p_T < 30 \text{ GeV}/c$ and $2.0 < y < 4.5$. Ratios between the cross-section measurements at 13 TeV and 8 TeV [18] are also presented. The measurements are compared with theoretical predictions based on NRQCD [24].

2 The LHCb detector and event selection

The LHCb detector [25, 26] is a single-arm forward spectrometer covering the pseudorapidity range $2 < \eta < 5$, designed for the study of particles containing b or c quarks. The detector includes a high-precision tracking system consisting of a silicon-strip vertex detector surrounding the pp interaction region [27], a large-area silicon-strip detector located upstream of a dipole magnet with a bending power of about 4 Tm, and three stations of silicon-strip detectors and straw drift tubes [28] placed downstream of the magnet. The tracking system provides a measurement of momentum, p , of charged particles with a relative uncertainty that varies from 0.5% at low momentum to 1.0% at $200 \text{ GeV}/c$. The minimum distance of a track to a primary vertex, the impact parameter, is

measured with a resolution of $(15 + 29/p_{\mathrm{T}}) \mu\mathrm{m}$, where p_{T} is expressed in GeV/c . Different types of charged hadrons are distinguished using information from two ring-imaging Cherenkov detectors [29]. Photons, electrons and hadrons are identified by a calorimeter system consisting of scintillating-pad (SPD) and preshower detectors, an electromagnetic calorimeter and a hadronic calorimeter. Muons are identified by a system composed of alternating layers of iron and multiwire proportional chambers [30].

The data sample used in this measurement corresponds to an integrated luminosity of $277 \pm 11 \mathrm{pb}^{-1}$ of pp collisions at a centre-of-mass energy of 13 TeV collected during 2015. The online event selection is performed by a trigger system [31] that consists of a hardware stage selecting dimuon candidates with the product of the transverse momenta of the muons greater than $(1.3 \mathrm{GeV}/c)^2$, followed by a two-stage software selection based on the information available after full event reconstruction. In the software trigger, two muons with $p > 6 \mathrm{GeV}/c$, $p_{\mathrm{T}} > 300 \mathrm{MeV}/c$ are selected to form a Υ candidate. These two muon candidates are required to form a common vertex [32] with an invariant mass $M > 4.7 \mathrm{GeV}/c^2$. To reject high-multiplicity events with a large number of pp interactions, a set of global event requirements [31] is applied, which includes the requirement that the number of hits in the SPD subdetector be less than 900. In between the first and second stages of the software trigger, the alignment and calibration of the detector is performed nearly in real-time [33] and updated constants are made available for the trigger. The same alignment and calibration information is propagated to the offline reconstruction, ensuring the consistency and high-quality of the tracking and particle identification information between the trigger and offline software. The identical performance of the online and offline reconstruction offers the opportunity to perform physics analyses directly using candidates reconstructed in the trigger [31, 34] as done in the present analysis.

After the trigger, the Υ candidates are further selected offline by requiring two well identified muon candidates with transverse momentum larger than $1 \mathrm{GeV}/c$, and momentum larger than $10 \mathrm{GeV}/c$. The invariant mass of the two muon candidates is required to be in the range $8.5 < M < 11.5 \mathrm{GeV}/c^2$. Furthermore, the muons are required to form a vertex with good fit quality.

The event-selection efficiencies are determined using simulated samples, which are generated using PYTHIA 8 [35] with a specific LHCb configuration [36]. The three Υ states are assumed to be produced unpolarised in this analysis. The decays of hadrons are described by EVTGEN [37], in which final-state radiation is simulated using PHOTOS [38]. The GEANT4 toolkit [39] is used to describe the interactions of the generated particles with the detector and its response.

3 Cross-section determination

The double-differential production cross-section times dimuon branching fraction (\mathcal{B}) is defined as

$$\frac{\mathrm{d}^2\sigma}{\mathrm{d}y\mathrm{d}p_{\mathrm{T}}} \times \mathcal{B}(\Upsilon \rightarrow \mu^+\mu^-) = \frac{N(p_{\mathrm{T}}, y)}{\mathcal{L} \times \varepsilon_{\mathrm{tot}}(p_{\mathrm{T}}, y) \times \Delta y \times \Delta p_{\mathrm{T}}}, \quad (1)$$

where $N(p_{\mathrm{T}}, y)$ and $\varepsilon_{\mathrm{tot}}(p_{\mathrm{T}}, y)$ are respectively the signal yields and the total efficiencies for $\Upsilon(1S)$, $\Upsilon(2S)$ and $\Upsilon(3S)$ states in the given kinematic bin, \mathcal{L} is the integrated luminosity, and Δp_{T} and Δy are the bin widths.

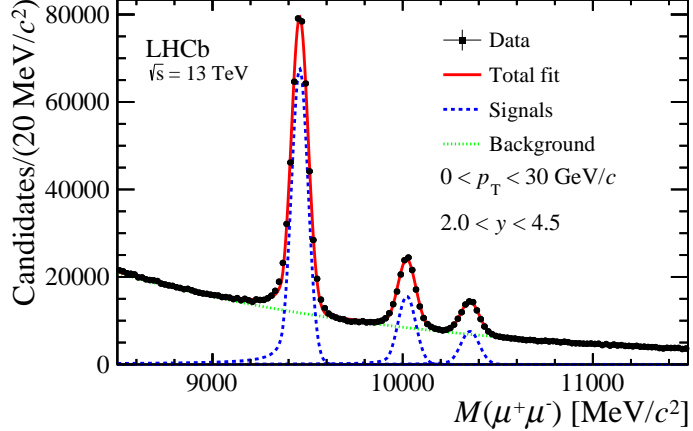


Figure 1: Dimuon invariant mass distribution of Υ candidates with $0 < p_T < 30 \text{ GeV}/c$ and $2.0 < y < 4.5$. The fit result with the Crystal Ball functions plus an exponential function is also shown. The black dots refer to the data, the blue dashed line refers to the three signals and the green dotted line refers to the background.

To determine the signal yields in each kinematic bin, an extended unbinned maximum-likelihood fit is performed to the dimuon invariant mass distribution of the selected candidates. The dimuon mass distribution is described by three Crystal Ball functions [40], one for each of the three Υ states, and the combinatorial background is described by an exponential function. In each bin, the tail parameters of the Crystal Ball functions are fixed as done in the previous analysis [16]. The mass and mass resolution of the $\Upsilon(1S)$ state are free parameters. For the $\Upsilon(2S)$ and $\Upsilon(3S)$ states, the mass differences with respect to the $\Upsilon(1S)$ state are fixed to the current world averages [41] and the ratios of the mass resolutions with respect to that of the $\Upsilon(1S)$ state are fixed to those in the simulated samples.

The invariant mass distribution of Υ candidates after all the selections in the range $0 < p_T < 30 \text{ GeV}/c$ and $2.0 < y < 4.5$ and the fit results are shown in Fig. 1. The total signal yields are $397\,841 \pm 796$ for the $\Upsilon(1S)$ state, $99\,790 \pm 469$ for the $\Upsilon(2S)$ state and $50\,677 \pm 381$ for the $\Upsilon(3S)$ state.

The total efficiency, ε_{tot} , in each bin is computed as the product of the detector geometrical acceptance and of the efficiencies related to particle reconstruction, event selection, muon identification and trigger. The detector acceptance, selection and trigger efficiencies are calculated using simulation. The tracking efficiency is obtained from simulation and corrected using a data-driven method [42] to improve its modelling in simulation samples. The muon identification efficiency is determined from simulation and calibrated with $J/\psi \rightarrow \mu^+\mu^-$ and $\phi \rightarrow \mu^+\mu^-$ data using a tag-and-probe method. The calibration samples in data are not sufficient to give precise tracking and muon identification efficiencies for the whole kinematic region.

4 Systematic uncertainties

Several sources of systematic uncertainties are associated with the determination of the signal yields, efficiencies, and integrated luminosity. They are reported in Table 1 and

Source	$\Upsilon(1S)$	$\Upsilon(2S)$	$\Upsilon(3S)$	Comment
Fit models	1.9	1.8	2.5	Correlated
Simulation statistics	0.4 – 4.6	0.5 – 5.1	0.5 – 4.4	Bin dependent
Global event requirements	0.6	0.6	0.6	Correlated
Trigger	3.9 – 9.8	3.9 – 9.8	3.9 – 9.8	Bin dependent
Tracking	(0.1 – 6.6) $\oplus(2 \times 0.8)$	(0.2 – 6.4) $\oplus(2 \times 0.8)$	(0.2 – 6.5) $\oplus(2 \times 0.8)$	Correlated
Muon identification	0.1 – 7.9	0.1 – 7.6	0.2 – 8.5	Correlated
Vertexing	0.2	0.2	0.2	Correlated
Kinematic spectrum	0.0 – 1.1	0.0 – 2.2	0.0 – 2.5	Bin dependent
Radiative tail	1.0	1.0	1.0	Correlated
Luminosity	3.9	3.9	3.9	Correlated
Total	6.2 – 14.3	6.2 – 14.6	6.4 – 14.9	Correlated

Table 1: Summary of the relative systematic uncertainties (in %) on the Υ production cross-sections times dimuon branching fractions. Some of the uncertainties are correlated between intervals. For the trigger, track reconstruction and muon identification efficiencies, the uncertainties are larger in the high rapidity region. The uncertainties on the tracking efficiency account for both the limited size of the control samples (first parenthesis) and the impact of different multiplicity between data and simulation on each track (second parenthesis).

described below. The dominant uncertainties are due to the trigger efficiency and the luminosity.

The uncertainty related to the fit model predominantly originates from the description of the signal tails caused by final-state radiation, and from the description of the background line shape. The former is studied by using the same fit model to describe the dimuon invariant-mass distribution of a mixed sample in which the signal is from the full simulation, and the background is generated with pseudoexperiments using the same shape and fraction as in the data. The latter is studied by replacing the exponential function with a second-order Chebyshev polynomial function. A combined relative uncertainty of 1.9% for the $\Upsilon(1S)$ state, 1.8% for the $\Upsilon(2S)$ state and 2.5% for the $\Upsilon(3S)$ state is assigned.

The efficiency of the global event requirements is found to be 100% in simulation, and 99.4% in data, with negligible statistical uncertainty. The difference, 0.6%, is assigned as systematic uncertainty.

The trigger efficiency uncertainty is computed using the same method as in the 7 TeV and 8 TeV analyses [18]. The dimuon hardware-trigger efficiency is studied with events triggered by the single-muon hardware trigger. The difference of this efficiency in data and simulated samples divided by that in simulation is assigned as the relative systematic uncertainty. The systematic uncertainty related to the global event requirements applied in the single-muon trigger, as well as other sources of uncertainties are assumed to be equal to those estimated in the inclusive $b\bar{b}$ cross-section measurements at 7 TeV and 13 TeV [43]. In total, the systematic uncertainty coming from trigger efficiencies is 3.9 – 9.8% for the three Υ states, depending on the kinematic bin.

The tracking efficiencies in simulation are corrected with a data-driven method using $J/\psi \rightarrow \mu^+\mu^-$ control samples. The number of SPD hits distributions in simulated samples are weighted to improve the agreement with data and an uncertainty of 0.8% per track is

assigned to account for a different multiplicity between data and simulation. The tracking efficiencies determined from simulated samples are corrected with the ratio of efficiencies in data and simulation. The uncertainty due to the finite size of the control samples is propagated to the final systematic uncertainty using a large number of pseudoexperiments and is 0.1 – 6.6% for the $\Upsilon(1S)$ state, 0.2 – 6.4% for the $\Upsilon(2S)$ state and 0.2 – 6.5% for the $\Upsilon(3S)$ state, depending on the kinematic bin. In total, the systematic uncertainty originating from the tracking efficiency is 1.6 – 6.8% for the $\Upsilon(1S)$ state, 1.6 – 6.6% for the $\Upsilon(2S)$ state and 1.6 – 6.7% for the $\Upsilon(3S)$ state, depending on the kinematic bin.

The muon identification efficiency is determined from simulation and calibrated with data using a tag-and-probe method. The single-muon identification efficiency is measured in intervals of p , η and event multiplicity. The statistical uncertainty due to the finite size of the calibration sample is propagated to the final results using pseudoexperiments. The uncertainty related to the kinematic binning scheme of the calibration samples is studied by changing the bin size. The uncertainty due to the kinematic correlations between the two muons, which is not considered in the efficiency calculation, is studied with simulated samples. The correlation is found to be negligible except for the most forward region, in which the two muons from the Υ decays have smaller opening angle. In total, the systematic uncertainty assigned to the muon identification efficiency is 0.1 – 7.9% for the $\Upsilon(1S)$ state, 0.1 – 7.6% for the $\Upsilon(2S)$ state and 0.2 – 8.5% for the $\Upsilon(3S)$ state, depending on the kinematic bin.

The systematic uncertainty on the signal efficiency of the vertex fit quality requirement is studied by comparing data and simulation. A relative difference of 0.2% is assigned for the three Υ states.

The kinematic distributions of Υ mesons in simulation and in data are slightly different within each kinematic bin due to the finite bin size in p_T and y , causing differences in efficiencies. This effect is studied by weighting the kinematic distributions of Υ states in simulation to match the distributions in data. All efficiencies are recalculated, and the relative differences of the total efficiency between the new and the nominal results are assigned as systematic uncertainties, which vary between 0.0 – 1.1% for the $\Upsilon(1S)$ state, 0.0 – 2.2% for the $\Upsilon(2S)$ state and 0.0 – 2.5% for the $\Upsilon(3S)$ state, depending on the kinematic bin.

A systematic uncertainty of 1.0% is assigned as a consequence of the limited precision on the modelling of the final-state radiation in the simulation, estimated as in the previous analysis [20].

The integrated luminosity is determined using the beam-gas imaging and van der Meer scan methods [44]. A relative uncertainty of 3.9% is assigned on the luminosity and propagated to the cross-sections.

5 Results

5.1 Cross-sections

The double-differential cross-sections multiplied by dimuon branching fractions for the $\Upsilon(1S)$, $\Upsilon(2S)$ and $\Upsilon(3S)$ states are shown in Fig. 2. The corresponding values are listed in Tables 2–4. By integrating the double-differential results over p_T (y), the differential cross-sections times dimuon branching fractions as functions of y (p_T) are shown in Fig. 3

for the three Υ states, with the theoretical predictions based on NRQCD [24] overlaid. The NRQCD predictions are in agreement with the experimental data at high p_T .

The total cross-sections multiplied by dimuon branching fractions for the three states integrated over the ranges of $0 < p_T < 15 \text{ GeV}/c$ and $2.0 < y < 4.5$ are measured to be

$$\begin{aligned}\mathcal{B}(\Upsilon(1S) \rightarrow \mu^+ \mu^-) \times \sigma(\Upsilon(1S), 0 < p_T < 15 \text{ GeV}/c, 2 < y < 4.5) &= 4687 \pm 10 \pm 294 \text{ pb}, \\ \mathcal{B}(\Upsilon(2S) \rightarrow \mu^+ \mu^-) \times \sigma(\Upsilon(2S), 0 < p_T < 15 \text{ GeV}/c, 2 < y < 4.5) &= 1134 \pm 6 \pm 71 \text{ pb}, \\ \mathcal{B}(\Upsilon(3S) \rightarrow \mu^+ \mu^-) \times \sigma(\Upsilon(3S), 0 < p_T < 15 \text{ GeV}/c, 2 < y < 4.5) &= 561 \pm 4 \pm 36 \text{ pb},\end{aligned}$$

where the first uncertainty is statistical and the second is systematic. The corresponding results as a function of pp centre-of-mass energy are shown in Fig. 4.

In this paper, results are obtained under the assumption of zero polarisation. The effects of possible Υ polarisation based on the LHCb measurements [19] in pp collisions at 7 TeV and 8 TeV are studied. The measurements show no large transverse or longitudinal polarisation over the accessible phase-space domain. The cross-sections increase up to 2.8% for the three Υ states when assuming the transverse polarisation of $\alpha = 0.1$, where α is the polarisation parameter in the helicity frame [45].

5.2 Cross-section ratios

The ratios of the differential production cross-sections multiplied by dimuon branching fractions between $\Upsilon(2S)$ and $\Upsilon(1S)$, $R_{2S/1S}$, and that between $\Upsilon(3S)$ and $\Upsilon(1S)$, $R_{3S/1S}$, are shown in Fig. 5.

In these ratios, the statistical uncertainties of the cross-sections and those due to the finite size of the simulated samples are assumed to be uncorrelated. The systematic uncertainties related to the signal yields and the efficiencies of the global event requirements, the trigger and the tracking are assumed to be 100% correlated between the different states.

The cross-sections times dimuon branching fractions measured at a centre-of-mass energy of 13 TeV presented in this paper are compared with the measurements at 8 TeV [18]. The ratios of double-differential cross-sections between 13 TeV and 8 TeV measurements, $R_{13/8}$, are shown in Fig. 6. The corresponding values are listed in Tables 5–7. The cross-section ratios between 13 TeV and 8 TeV versus p_T integrated over y , and versus y integrated over p_T are shown in Fig. 7.

In the ratios, the systematic uncertainties originating from the fit model, global event requirements and kinematic spectrum are assumed to be uncorrelated. Those from trigger, muon identification, tracking correction and luminosity are partially correlated. The systematic uncertainty from final-state radiation is assumed to be 100% correlated.

6 Conclusion

A study of the production of $\Upsilon(1S)$, $\Upsilon(2S)$ and $\Upsilon(3S)$ mesons in proton-proton collisions at the centre-of-mass energy $\sqrt{s} = 13 \text{ TeV}$ is reported. The differential cross-sections times dimuon branching fractions of Υ mesons are measured as functions of p_T and y , in the kinematic range $0 < p_T < 30 \text{ GeV}/c$ and $2.0 < y < 4.5$. The production cross-section ratios of $\Upsilon(2S)$ and $\Upsilon(3S)$ mesons with respect to the $\Upsilon(1S)$ meson are given in intervals

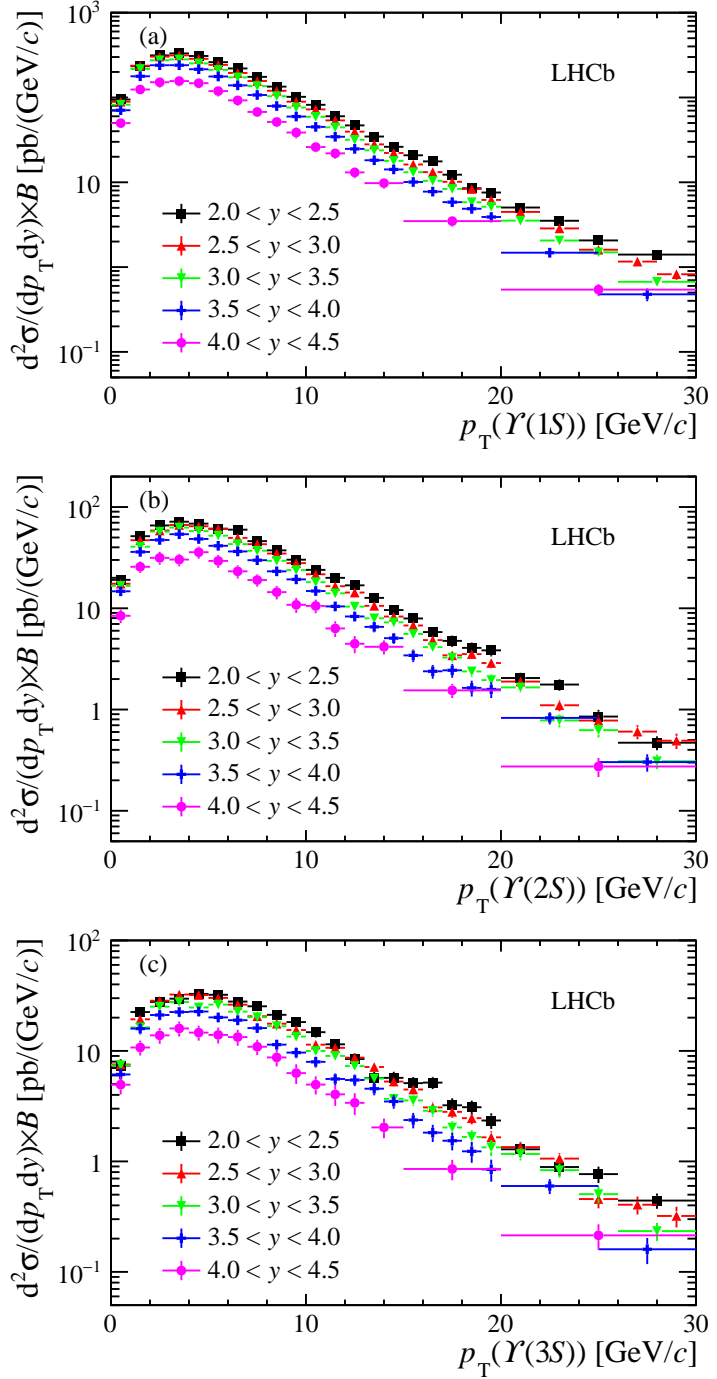


Figure 2: Double-differential cross-sections multiplied by dimuon branching fractions as a function of p_T in intervals of y for the (a) $\Upsilon(1S)$, (b) $\Upsilon(2S)$ and (c) $\Upsilon(3S)$ mesons. Statistical and systematic uncertainties are added in quadrature.

of p_T and y . The ratios of the production cross-sections with respect to those measured at $\sqrt{s} = 8$ TeV are also presented.

The results of differential cross-sections times dimuon branching fractions as a function of p_T integrated over y between 2.0 and 4.5 are compared with predictions based on NRQCD. These predictions provide a good description of the experimental data at high

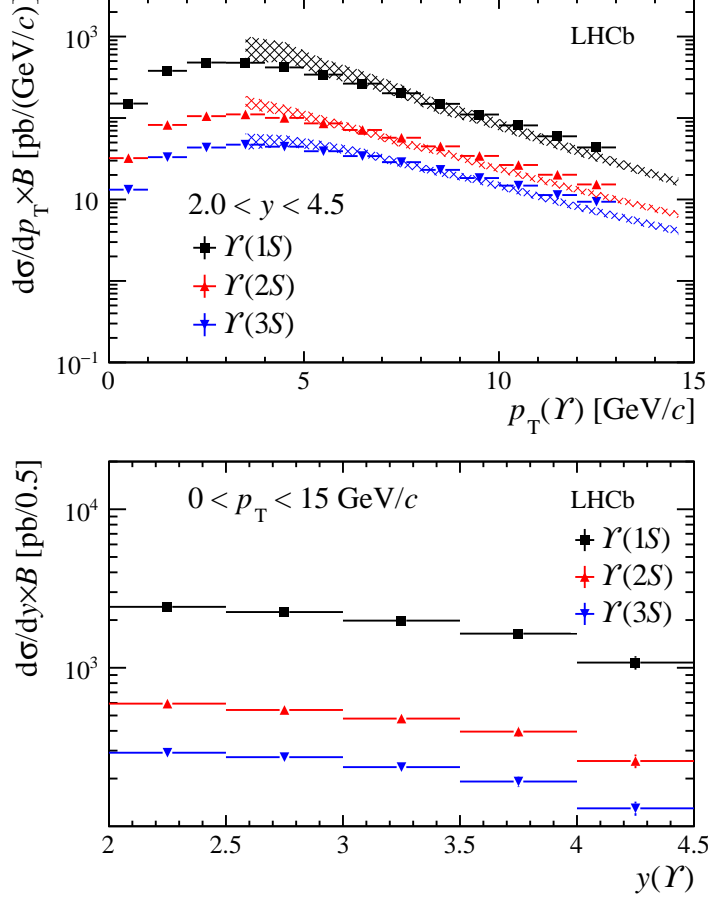


Figure 3: Differential cross-sections multiplied by dimuon branching fractions for the $\Upsilon(1S)$ (black solid squares), $\Upsilon(2S)$ (red upward triangles) and $\Upsilon(3S)$ (blue downward triangles) states (top) versus p_T integrated over y between 2.0 and 4.5 and (bottom) versus y integrated over p_T from 0 to 15 GeV/c. Statistical and systematic uncertainties are added in quadrature. Predictions from NRQCD [24] for the $\Upsilon(1S)$ (black grid shading), $\Upsilon(2S)$ (red grid shading) and $\Upsilon(3S)$ (blue grid shading) states are overlaid in the top plot.

p_T for all the three Υ states.

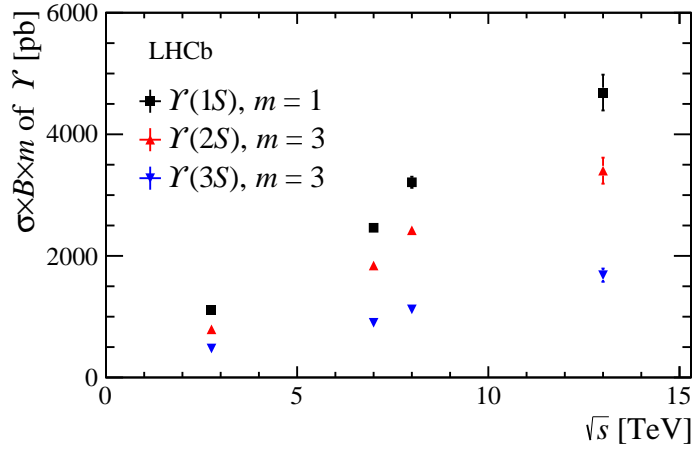


Figure 4: The production cross-sections multiplied by dimuon branching fractions integrated over $0 < p_T < 15 \text{ GeV}/c$ and $2.0 < y < 4.5$ versus centre-of-mass energy of pp collisions for the $\Upsilon(1S)$ (black solid squares), $\Upsilon(2S)$ (red upward triangles) and $\Upsilon(3S)$ (blue downward triangles) states. Each set of measurements is offset by a multiplicative factor m , which is shown on the plot. Statistical and systematic uncertainties are added in quadrature.

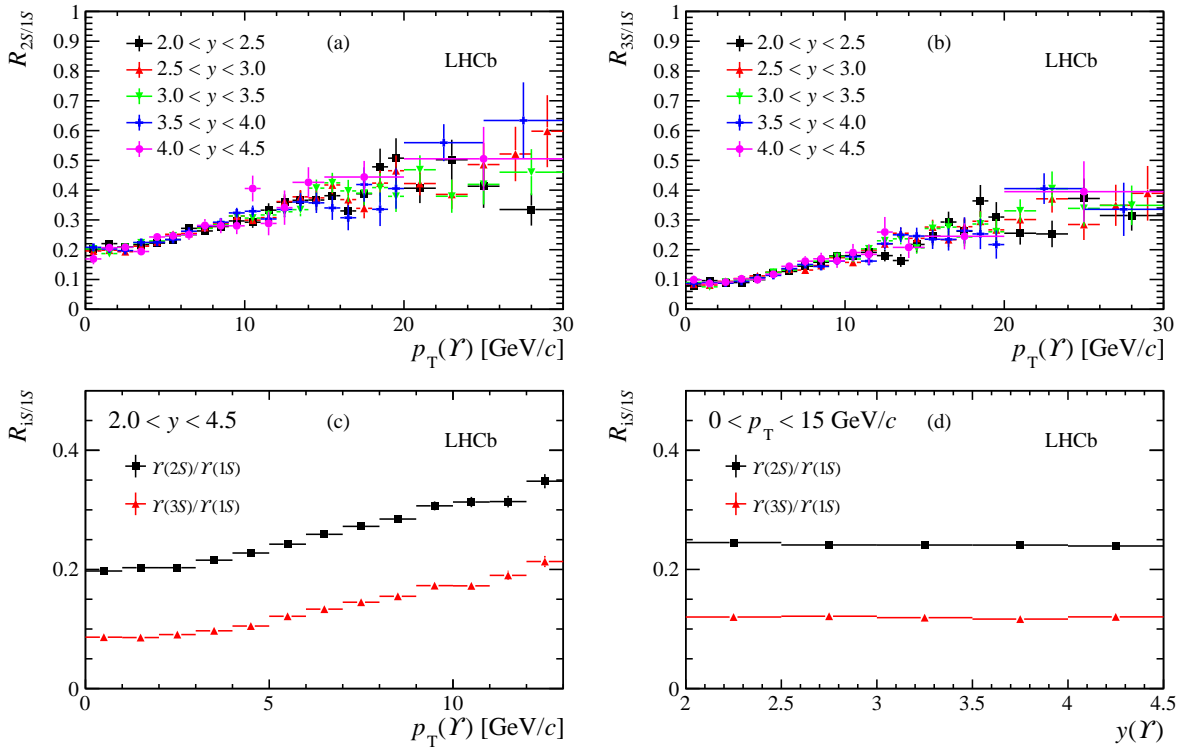


Figure 5: Ratios of double-differential cross-sections times dimuon branching fractions for (a) $\Upsilon(2S)$ to $\Upsilon(1S)$ and (b) $\Upsilon(3S)$ to $\Upsilon(1S)$. Ratios of differential cross-sections times dimuon branching fractions (c) versus p_T integrated over y and (d) versus y integrated over p_T for $\Upsilon(2S)$ to $\Upsilon(1S)$ (black solid squares) and $\Upsilon(3S)$ to $\Upsilon(1S)$ (red upward triangles). Statistical and systematic uncertainties are added in quadrature.

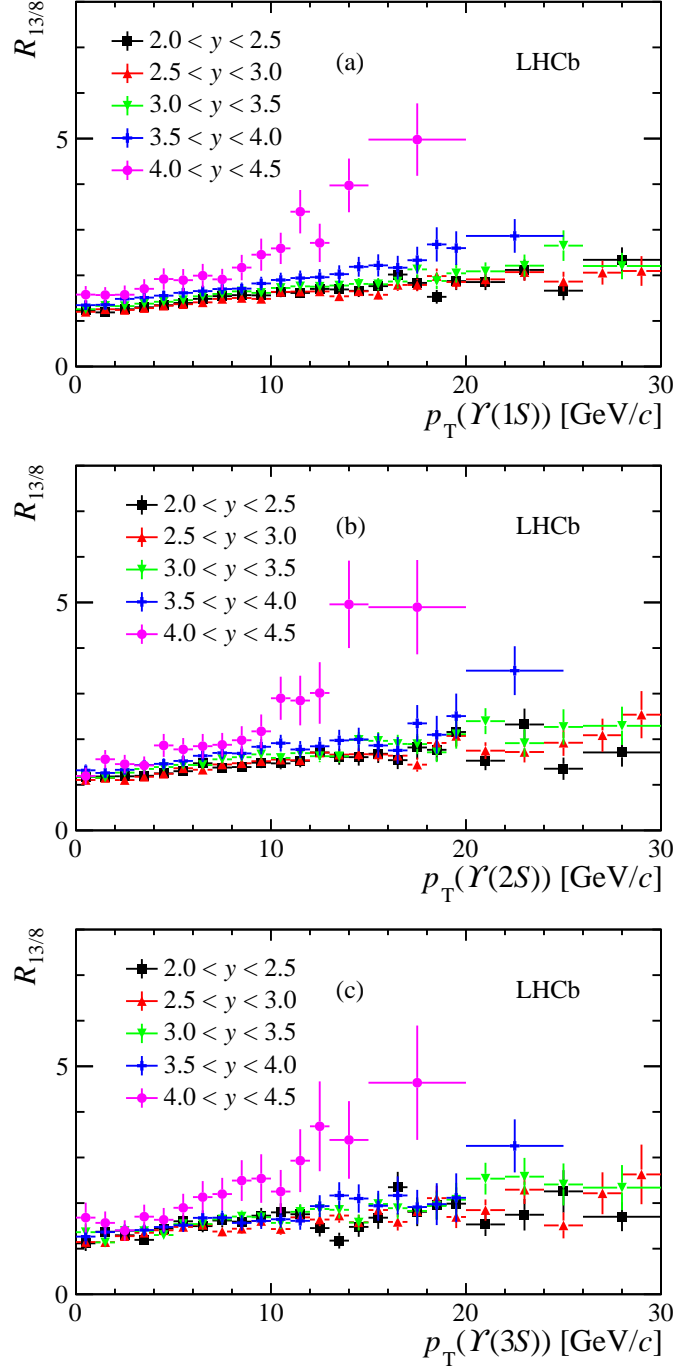


Figure 6: Ratios of double-differential cross-sections between 13 TeV and 8 TeV measurements versus p_T in intervals of y for the (a) $\Upsilon(1S)$, (b) $\Upsilon(2S)$ and (c) $\Upsilon(3S)$ states. Statistical and systematic uncertainties are added in quadrature.

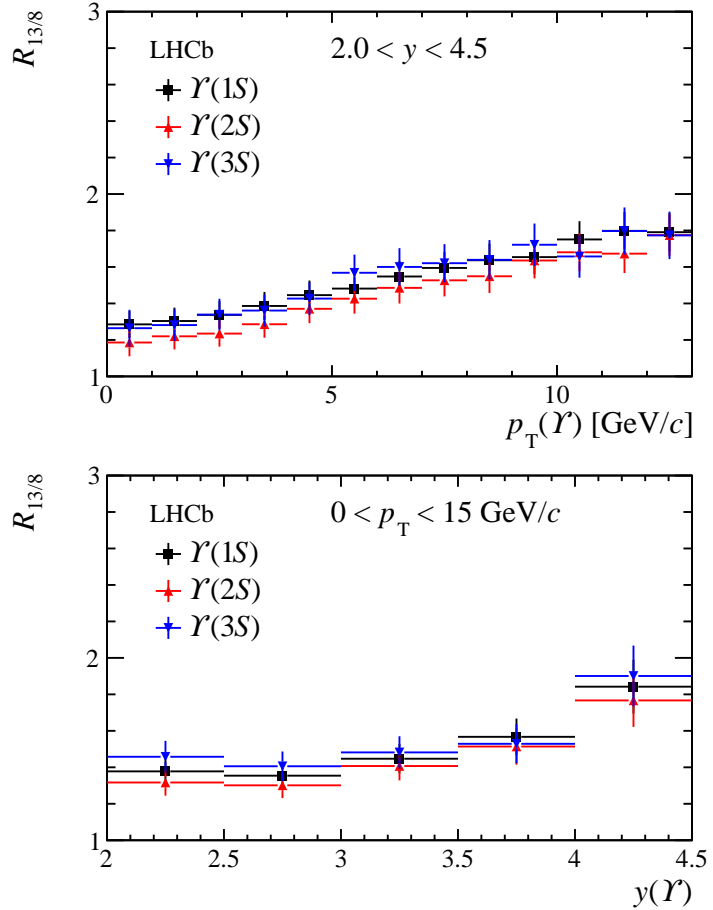


Figure 7: Ratios of differential cross-sections between 13 TeV and 8 TeV measurements (top) versus p_T integrated over y and (bottom) versus y integrated over p_T for the $\Upsilon(1S)$ (black solid squares), $\Upsilon(2S)$ (red upward triangles) and $\Upsilon(3S)$ (blue downward triangles) states. Statistical and systematic uncertainties are added in quadrature.

p_T [GeV/c]	$2.0 < y < 2.5$	$2.5 < y < 3.0$	$3.0 < y < 3.5$	$3.5 < y < 4.0$	$4.0 < y < 4.5$
0–1	94.75 ± 2.44 ± 6.27	89.26 ± 1.65 ± 5.65	82.21 ± 1.65 ± 5.63	70.76 ± 1.55 ± 6.10	49.85 ± 1.74 ± 5.94
1–2	233.67 ± 3.83 ± 15.52	236.95 ± 2.72 ± 14.94	216.85 ± 2.61 ± 14.87	177.87 ± 2.47 ± 16.12	124.19 ± 2.68 ± 14.27
2–3	313.67 ± 4.40 ± 20.72	303.07 ± 3.14 ± 18.95	274.80 ± 2.89 ± 18.39	240.07 ± 2.88 ± 20.28	151.23 ± 2.94 ± 20.38
3–4	330.78 ± 4.51 ± 22.11	313.85 ± 3.22 ± 19.58	281.00 ± 2.90 ± 18.17	240.17 ± 2.84 ± 18.96	156.12 ± 3.04 ± 20.26
4–5	308.47 ± 4.36 ± 20.08	285.77 ± 3.09 ± 18.01	251.96 ± 2.70 ± 16.26	215.22 ± 2.71 ± 17.63	147.40 ± 3.00 ± 18.69
5–6	261.01 ± 4.05 ± 17.44	242.35 ± 2.86 ± 15.04	211.58 ± 2.50 ± 13.80	176.79 ± 2.43 ± 13.91	118.96 ± 2.68 ± 16.00
6–7	219.98 ± 3.74 ± 13.90	194.56 ± 2.51 ± 12.11	172.49 ± 2.20 ± 11.10	138.96 ± 2.16 ± 11.22	92.48 ± 2.41 ± 12.40
7–8	175.08 ± 3.34 ± 11.48	156.34 ± 2.18 ± 9.76	136.22 ± 1.90 ± 8.62	107.01 ± 1.87 ± 8.15	67.50 ± 2.05 ± 8.26
8–9	134.33 ± 2.86 ± 8.69	119.99 ± 1.86 ± 7.49	103.59 ± 1.58 ± 6.65	79.26 ± 1.57 ± 6.62	51.49 ± 1.85 ± 6.58
9–10	101.78 ± 2.46 ± 6.58	89.18 ± 1.54 ± 5.63	76.04 ± 1.34 ± 4.98	59.62 ± 1.33 ± 5.06	38.61 ± 1.59 ± 5.52
10–11	81.97 ± 2.14 ± 5.57	72.34 ± 1.34 ± 4.54	59.17 ± 1.16 ± 3.92	44.99 ± 1.13 ± 3.88	26.02 ± 1.30 ± 3.16
11–12	60.06 ± 1.78 ± 4.12	53.65 ± 1.14 ± 3.38	44.40 ± 0.99 ± 2.96	34.43 ± 0.97 ± 2.98	21.94 ± 1.17 ± 2.79
12–13	46.88 ± 1.54 ± 3.25	39.55 ± 0.98 ± 2.50	31.71 ± 0.83 ± 2.12	24.76 ± 0.82 ± 2.24	13.07 ± 0.93 ± 1.69
13–14	34.64 ± 1.30 ± 2.44	28.00 ± 0.79 ± 1.78	23.81 ± 0.71 ± 1.61	18.20 ± 0.70 ± 1.67	9.77 ± 0.53 ± 1.24
14–15	26.20 ± 1.10 ± 1.85	22.15 ± 0.68 ± 1.42	17.87 ± 0.61 ± 1.23	14.18 ± 0.60 ± 1.30	
15–16	20.81 ± 0.97 ± 1.49	16.20 ± 0.58 ± 1.05	13.14 ± 0.51 ± 0.91	10.07 ± 0.51 ± 1.01	
16–17	17.64 ± 0.87 ± 1.27	13.17 ± 0.53 ± 0.87	10.41 ± 0.46 ± 0.75	7.76 ± 0.46 ± 0.81	
17–18	12.29 ± 0.65 ± 0.89	10.13 ± 0.45 ± 0.68	8.35 ± 0.41 ± 0.61	5.83 ± 0.39 ± 0.62	3.48 ± 0.20 ± 0.44
18–19	8.50 ± 0.53 ± 0.63	8.33 ± 0.42 ± 0.58	5.82 ± 0.35 ± 0.44	4.88 ± 0.37 ± 0.54	
19–20	7.57 ± 0.50 ± 0.58	6.19 ± 0.34 ± 0.43	5.15 ± 0.32 ± 0.39	3.90 ± 0.31 ± 0.43	
20–21	5.04 ± 0.29 ± 0.37	4.47 ± 0.21 ± 0.31	3.53 ± 0.18 ± 0.27		
21–22					
22–23	3.52 ± 0.24 ± 0.27	2.86 ± 0.17 ± 0.21	2.06 ± 0.14 ± 0.17	1.48 ± 0.09 ± 0.17	
23–24					
24–25	2.06 ± 0.17 ± 0.16	1.60 ± 0.12 ± 0.12	1.49 ± 0.12 ± 0.13		0.54 ± 0.06 ± 0.07
25–26					
26–27		1.16 ± 0.10 ± 0.10	0.67 ± 0.06 ± 0.06	0.48 ± 0.05 ± 0.06	
27–28	1.40 ± 0.10 ± 0.11		0.82 ± 0.09 ± 0.07		
28–29					
29–30					

Table 2: Double-differential cross-sections times dimuon branching fraction in different bins of p_T and y for $\Upsilon(1S)$ (in pb). The first uncertainty is statistical and the second is systematic.

p_T [GeV/c]	$2.0 < y < 2.5$	$2.5 < y < 3.0$	$3.0 < y < 3.5$	$3.5 < y < 4.0$	$4.0 < y < 4.5$
0–1	19.09 ± 1.26 ± 1.29	17.48 ± 0.87 ± 1.11	16.64 ± 0.92 ± 1.14	14.71 ± 0.83 ± 1.26	8.43 ± 0.79 ± 1.02
1–2	51.52 ± 2.06 ± 3.43	47.02 ± 1.45 ± 2.96	40.56 ± 1.42 ± 2.77	36.04 ± 1.33 ± 3.25	25.69 ± 1.38 ± 3.04
2–3	65.75 ± 2.33 ± 4.33	58.61 ± 1.65 ± 3.66	57.16 ± 1.63 ± 3.85	47.30 ± 1.52 ± 4.04	31.50 ± 1.49 ± 4.31
3–4	71.64 ± 2.44 ± 4.76	66.47 ± 1.78 ± 4.14	62.67 ± 1.65 ± 4.06	53.90 ± 1.59 ± 4.38	30.28 ± 1.52 ± 4.01
4–5	68.54 ± 2.36 ± 4.43	64.62 ± 1.75 ± 4.06	57.78 ± 1.53 ± 3.72	48.37 ± 1.50 ± 4.04	35.79 ± 1.65 ± 4.62
5–6	61.05 ± 2.23 ± 4.05	61.03 ± 1.68 ± 3.78	52.15 ± 1.45 ± 3.39	41.41 ± 1.37 ± 3.31	29.36 ± 1.54 ± 3.96
6–7	59.77 ± 2.22 ± 3.78	49.55 ± 1.50 ± 3.08	43.04 ± 1.29 ± 2.76	36.43 ± 1.26 ± 2.98	23.17 ± 1.39 ± 3.17
7–8	46.04 ± 1.94 ± 3.03	42.95 ± 1.32 ± 2.68	37.01 ± 1.12 ± 2.34	29.84 ± 1.14 ± 2.33	19.00 ± 1.25 ± 2.35
8–9	37.33 ± 1.76 ± 2.43	34.72 ± 1.14 ± 2.16	29.41 ± 0.95 ± 1.88	23.17 ± 0.97 ± 1.99	14.44 ± 1.10 ± 1.91
9–10	30.18 ± 1.52 ± 1.98	27.93 ± 0.98 ± 1.76	23.81 ± 0.81 ± 1.57	19.29 ± 0.84 ± 1.64	10.82 ± 0.92 ± 1.57
10–11	23.97 ± 1.32 ± 1.66	21.65 ± 0.83 ± 1.37	18.12 ± 0.71 ± 1.20	14.81 ± 0.71 ± 1.27	10.55 ± 0.91 ± 1.33
11–12	19.99 ± 1.17 ± 1.41	16.51 ± 0.69 ± 1.04	14.06 ± 0.60 ± 0.94	10.44 ± 0.59 ± 0.93	6.32 ± 0.76 ± 0.81
12–13	16.85 ± 1.03 ± 1.19	14.30 ± 0.61 ± 0.90	10.38 ± 0.51 ± 0.71	8.30 ± 0.52 ± 0.75	4.46 ± 0.64 ± 0.57
13–14	12.67 ± 0.94 ± 0.92	10.57 ± 0.53 ± 0.67	7.96 ± 0.44 ± 0.54	6.55 ± 0.44 ± 0.62	4.16 ± 0.40 ± 0.53
14–15	9.61 ± 0.75 ± 0.71	8.29 ± 0.46 ± 0.53	7.27 ± 0.41 ± 0.51	5.07 ± 0.39 ± 0.47	
15–16	7.93 ± 0.66 ± 0.58	6.76 ± 0.40 ± 0.44	5.58 ± 0.35 ± 0.39	3.43 ± 0.34 ± 0.35	
16–17	5.82 ± 0.55 ± 0.43	4.85 ± 0.34 ± 0.32	4.14 ± 0.31 ± 0.30	2.39 ± 0.27 ± 0.25	
17–18	4.77 ± 0.48 ± 0.37	3.43 ± 0.28 ± 0.23	3.26 ± 0.27 ± 0.24	2.44 ± 0.27 ± 0.27	
18–19	4.07 ± 0.42 ± 0.31	3.53 ± 0.28 ± 0.24	2.38 ± 0.23 ± 0.18	1.64 ± 0.23 ± 0.18	
19–20	3.84 ± 0.39 ± 0.31	2.88 ± 0.25 ± 0.20	1.95 ± 0.22 ± 0.15	1.58 ± 0.20 ± 0.19	
20–21	2.05 ± 0.20 ± 0.16	1.89 ± 0.14 ± 0.13	1.65 ± 0.13 ± 0.13		
21–22					
22–23	1.77 ± 0.18 ± 0.14	1.10 ± 0.11 ± 0.08	0.78 ± 0.09 ± 0.06	0.83 ± 0.07 ± 0.09	
23–24					
24–25	0.85 ± 0.12 ± 0.07	0.78 ± 0.09 ± 0.06	0.63 ± 0.08 ± 0.05		0.27 ± 0.05 ± 0.04
25–26					
26–27		0.61 ± 0.08 ± 0.05		0.30 ± 0.05 ± 0.04	
27–28	0.47 ± 0.06 ± 0.04		0.31 ± 0.04 ± 0.03		
28–29		0.49 ± 0.07 ± 0.04			
29–30					

Table 3: Double-differential cross-sections times dimuon branching fraction in different bins of p_T and y for $\Upsilon(2S)$ (in pb). The first uncertainty is statistical and the second is systematic.

p_T [GeV/c]	$2.0 < y < 2.5$	$2.5 < y < 3.0$	$3.0 < y < 3.5$	$3.5 < y < 4.0$	$4.0 < y < 4.5$
0–1	$7.37 \pm 0.91 \pm 0.51$	$7.54 \pm 0.66 \pm 0.50$	$7.41 \pm 0.78 \pm 0.52$	$6.12 \pm 0.64 \pm 0.55$	$4.94 \pm 0.67 \pm 0.62$
1–2	$22.47 \pm 1.58 \pm 1.54$	$19.32 \pm 1.10 \pm 1.26$	$16.34 \pm 1.13 \pm 1.16$	$15.91 \pm 1.05 \pm 1.48$	$10.74 \pm 0.96 \pm 1.35$
2–3	$27.76 \pm 1.75 \pm 1.90$	$28.45 \pm 1.32 \pm 1.84$	$25.14 \pm 1.32 \pm 1.74$	$21.13 \pm 1.21 \pm 1.85$	$13.83 \pm 1.12 \pm 1.92$
3–4	$29.69 \pm 1.81 \pm 2.04$	$32.38 \pm 1.42 \pm 2.09$	$27.69 \pm 1.31 \pm 1.86$	$22.49 \pm 1.24 \pm 1.88$	$15.97 \pm 1.22 \pm 2.17$
4–5	$32.80 \pm 1.85 \pm 2.20$	$32.05 \pm 1.42 \pm 2.09$	$24.71 \pm 1.19 \pm 1.65$	$22.72 \pm 1.19 \pm 1.94$	$14.63 \pm 1.21 \pm 1.91$
5–6	$32.21 \pm 1.81 \pm 2.21$	$30.17 \pm 1.34 \pm 1.94$	$26.25 \pm 1.16 \pm 1.77$	$20.10 \pm 1.10 \pm 1.69$	$13.96 \pm 1.18 \pm 1.96$
6–7	$27.96 \pm 1.74 \pm 1.82$	$26.21 \pm 1.23 \pm 1.69$	$22.66 \pm 1.06 \pm 1.51$	$18.97 \pm 1.03 \pm 1.61$	$13.34 \pm 1.16 \pm 1.87$
7–8	$25.34 \pm 1.62 \pm 1.71$	$20.59 \pm 1.05 \pm 1.33$	$20.17 \pm 0.90 \pm 1.32$	$16.09 \pm 0.93 \pm 1.28$	$10.90 \pm 1.05 \pm 1.38$
8–9	$21.21 \pm 1.45 \pm 1.42$	$17.63 \pm 0.92 \pm 1.14$	$16.74 \pm 0.78 \pm 1.11$	$11.39 \pm 0.77 \pm 1.01$	$8.73 \pm 0.96 \pm 1.14$
9–10	$18.24 \pm 1.27 \pm 1.22$	$15.46 \pm 0.81 \pm 1.01$	$13.48 \pm 0.67 \pm 0.92$	$9.65 \pm 0.65 \pm 0.85$	$6.29 \pm 0.86 \pm 0.94$
10–11	$14.77 \pm 1.17 \pm 1.04$	$11.39 \pm 0.67 \pm 0.74$	$9.99 \pm 0.57 \pm 0.69$	$7.96 \pm 0.57 \pm 0.70$	$4.96 \pm 0.69 \pm 0.62$
11–12	$11.48 \pm 0.99 \pm 0.82$	$10.66 \pm 0.59 \pm 0.70$	$9.00 \pm 0.52 \pm 0.62$	$5.57 \pm 0.46 \pm 0.49$	$4.04 \pm 0.69 \pm 0.52$
12–13	$8.45 \pm 0.84 \pm 0.61$	$8.69 \pm 0.53 \pm 0.57$	$7.29 \pm 0.44 \pm 0.51$	$5.45 \pm 0.43 \pm 0.49$	$3.39 \pm 0.59 \pm 0.46$
13–14	$5.67 \pm 0.69 \pm 0.41$	$7.15 \pm 0.45 \pm 0.47$	$5.63 \pm 0.38 \pm 0.40$	$4.55 \pm 0.40 \pm 0.43$	$2.03 \pm 0.32 \pm 0.26$
14–15	$5.70 \pm 0.64 \pm 0.42$	$5.28 \pm 0.38 \pm 0.35$	$3.68 \pm 0.31 \pm 0.26$	$3.49 \pm 0.35 \pm 0.34$	
15–16	$5.11 \pm 0.57 \pm 0.38$	$4.47 \pm 0.35 \pm 0.30$	$3.56 \pm 0.30 \pm 0.26$	$2.37 \pm 0.29 \pm 0.24$	
16–17	$5.17 \pm 0.53 \pm 0.39$	$3.08 \pm 0.29 \pm 0.21$	$2.87 \pm 0.27 \pm 0.21$	$1.82 \pm 0.25 \pm 0.20$	
17–18	$3.22 \pm 0.44 \pm 0.25$	$2.81 \pm 0.26 \pm 0.19$	$2.03 \pm 0.23 \pm 0.15$	$1.54 \pm 0.23 \pm 0.16$	
18–19	$3.09 \pm 0.38 \pm 0.25$	$2.46 \pm 0.24 \pm 0.17$	$1.67 \pm 0.21 \pm 0.13$	$1.23 \pm 0.22 \pm 0.14$	
19–20	$2.34 \pm 0.33 \pm 0.19$	$1.65 \pm 0.19 \pm 0.12$	$1.34 \pm 0.19 \pm 0.11$	$0.85 \pm 0.16 \pm 0.10$	
20–21	$1.29 \pm 0.17 \pm 0.10$	$1.35 \pm 0.12 \pm 0.09$	$1.17 \pm 0.11 \pm 0.09$		
21–22					
22–23	$0.89 \pm 0.14 \pm 0.07$	$1.06 \pm 0.11 \pm 0.08$	$0.83 \pm 0.10 \pm 0.07$	$0.60 \pm 0.06 \pm 0.07$	
23–24					
24–25	$0.77 \pm 0.11 \pm 0.06$	$0.46 \pm 0.07 \pm 0.03$	$0.51 \pm 0.07 \pm 0.04$		$0.21 \pm 0.05 \pm 0.03$
25–26					
26–27		$0.41 \pm 0.07 \pm 0.03$			$0.16 \pm 0.04 \pm 0.02$
27–28					
28–29	$0.44 \pm 0.06 \pm 0.04$		$0.23 \pm 0.04 \pm 0.03$		
29–30					

Table 4: Double-differential cross-sections times dimuon branching fraction in different bins of p_T and y for $\Upsilon(3S)$ (in pb). The first uncertainty is statistical and the second is systematic.

p_T [GeV/c]	2.0 < y < 2.5	2.5 < y < 3.0	3.0 < y < 3.5	3.5 < y < 4.0	4.0 < y < 4.5
0–1	1.231 ± 0.081	1.200 ± 0.071	1.257 ± 0.081	1.346 ± 0.109	1.578 ± 0.188
1–2	1.187 ± 0.072	1.256 ± 0.070	1.330 ± 0.082	1.354 ± 0.113	1.568 ± 0.174
2–3	1.256 ± 0.075	1.241 ± 0.069	1.325 ± 0.080	1.484 ± 0.114	1.575 ± 0.203
3–4	1.299 ± 0.078	1.282 ± 0.070	1.379 ± 0.080	1.512 ± 0.109	1.704 ± 0.211
4–5	1.345 ± 0.079	1.334 ± 0.074	1.420 ± 0.082	1.555 ± 0.116	1.919 ± 0.235
5–6	1.393 ± 0.085	1.368 ± 0.076	1.455 ± 0.085	1.616 ± 0.117	1.894 ± 0.245
6–7	1.484 ± 0.087	1.408 ± 0.078	1.540 ± 0.089	1.654 ± 0.124	1.993 ± 0.258
7–8	1.544 ± 0.095	1.483 ± 0.083	1.591 ± 0.091	1.700 ± 0.120	1.912 ± 0.231
8–9	1.566 ± 0.096	1.504 ± 0.086	1.649 ± 0.096	1.709 ± 0.133	2.171 ± 0.279
9–10	1.561 ± 0.098	1.484 ± 0.086	1.616 ± 0.098	1.822 ± 0.147	2.453 ± 0.353
10–11	1.633 ± 0.112	1.637 ± 0.097	1.723 ± 0.106	1.899 ± 0.160	2.592 ± 0.343
11–12	1.614 ± 0.112	1.644 ± 0.098	1.759 ± 0.113	1.941 ± 0.165	3.396 ± 0.476
12–13	1.702 ± 0.122	1.648 ± 0.102	1.752 ± 0.115	1.959 ± 0.179	2.712 ± 0.421
13–14	1.691 ± 0.130	1.540 ± 0.099	1.777 ± 0.123	2.026 ± 0.194	
14–15	1.660 ± 0.136	1.651 ± 0.109	1.812 ± 0.130	2.188 ± 0.217	
15–16	1.763 ± 0.150	1.573 ± 0.110	1.805 ± 0.136	2.219 ± 0.243	
16–17	2.018 ± 0.174	1.790 ± 0.132	1.865 ± 0.151	2.168 ± 0.260	
17–18	1.834 ± 0.170	1.790 ± 0.138	2.131 ± 0.183	2.332 ± 0.296	
18–19	1.529 ± 0.150	1.984 ± 0.166	1.877 ± 0.180	2.679 ± 0.376	
19–20	1.874 ± 0.197	1.854 ± 0.164	2.044 ± 0.205	2.598 ± 0.369	
20–21	1.853 ± 0.176	1.912 ± 0.157	2.088 ± 0.196		
21–22				2.865 ± 0.369	
22–23	2.119 ± 0.230	2.071 ± 0.191	2.212 ± 0.244		
23–24					
24–25					
25–26	1.664 ± 0.210	1.863 ± 0.216	2.652 ± 0.335		
26–27					
27–28	2.340 ± 0.274	2.059 ± 0.262	2.205 ± 0.289		
28–29		2.096 ± 0.326			
29–30					

Table 5: The cross-section ratios between 13 TeV and 8 TeV in different bins of p_T and y for $\Upsilon(1S)$.

p_T [GeV/c]	2.0 < y < 2.5	2.5 < y < 3.0	3.0 < y < 3.5	3.5 < y < 4.0	4.0 < y < 4.5
0–1	1.177 ± 0.114	1.106 ± 0.086	1.177 ± 0.100	1.318 ± 0.128	1.194 ± 0.185
1–2	1.182 ± 0.086	1.150 ± 0.073	1.155 ± 0.082	1.260 ± 0.115	1.560 ± 0.201
2–3	1.187 ± 0.082	1.105 ± 0.068	1.267 ± 0.085	1.329 ± 0.112	1.454 ± 0.203
3–4	1.198 ± 0.083	1.177 ± 0.071	1.348 ± 0.086	1.433 ± 0.116	1.426 ± 0.196
4–5	1.251 ± 0.085	1.243 ± 0.076	1.390 ± 0.087	1.460 ± 0.121	1.864 ± 0.252
5–6	1.299 ± 0.092	1.363 ± 0.084	1.436 ± 0.093	1.524 ± 0.124	1.777 ± 0.249
6–7	1.472 ± 0.106	1.330 ± 0.084	1.433 ± 0.093	1.636 ± 0.138	1.847 ± 0.268
7–8	1.379 ± 0.102	1.446 ± 0.092	1.559 ± 0.101	1.699 ± 0.140	1.878 ± 0.260
8–9	1.390 ± 0.108	1.473 ± 0.097	1.605 ± 0.106	1.689 ± 0.152	1.978 ± 0.308
9–10	1.485 ± 0.120	1.518 ± 0.102	1.667 ± 0.115	1.834 ± 0.167	2.173 ± 0.370
10–11	1.470 ± 0.130	1.553 ± 0.110	1.589 ± 0.115	1.913 ± 0.184	2.899 ± 0.473
11–12	1.526 ± 0.142	1.538 ± 0.111	1.694 ± 0.132	1.775 ± 0.185	2.848 ± 0.545
12–13	1.709 ± 0.162	1.707 ± 0.126	1.627 ± 0.132	1.845 ± 0.203	3.014 ± 0.675
13–14	1.612 ± 0.173	1.662 ± 0.133	1.625 ± 0.144	1.974 ± 0.233	
14–15	1.607 ± 0.186	1.671 ± 0.143	1.986 ± 0.175	1.995 ± 0.257	
15–16	1.681 ± 0.201	1.666 ± 0.147	1.964 ± 0.192	1.863 ± 0.268	
16–17	1.541 ± 0.196	1.639 ± 0.161	1.897 ± 0.201	1.754 ± 0.294	
17–18	1.819 ± 0.253	1.442 ± 0.155	1.894 ± 0.221	2.348 ± 0.402	
18–19	1.768 ± 0.246	1.918 ± 0.210	1.713 ± 0.215	2.098 ± 0.414	
19–20	2.158 ± 0.307	2.073 ± 0.243	2.110 ± 0.317	2.507 ± 0.494	
20–21	1.529 ± 0.208	1.749 ± 0.184	2.396 ± 0.284		
21–22					
22–23	2.323 ± 0.349	1.720 ± 0.229	1.914 ± 0.304	3.504 ± 0.536	
23–24					
24–25					
25–26	1.353 ± 0.244	1.923 ± 0.288	2.269 ± 0.387		
26–27					
27–28		2.088 ± 0.364			
28–29	1.710 ± 0.312		2.294 ± 0.420		
29–30		2.538 ± 0.517			

Table 6: The cross-section ratios between 13 TeV and 8 TeV in different bins of p_T and y for $\Upsilon(2S)$.

p_T [GeV/c]	2.0 < y < 2.5	2.5 < y < 3.0	3.0 < y < 3.5	3.5 < y < 4.0	4.0 < y < 4.5
0–1	1.117 ± 0.167	1.145 ± 0.126	1.362 ± 0.174	1.265 ± 0.173	1.681 ± 0.328
1–2	1.372 ± 0.135	1.143 ± 0.095	1.138 ± 0.109	1.364 ± 0.152	1.566 ± 0.251
2–3	1.294 ± 0.119	1.275 ± 0.096	1.389 ± 0.116	1.397 ± 0.139	1.399 ± 0.223
3–4	1.193 ± 0.107	1.349 ± 0.099	1.386 ± 0.108	1.409 ± 0.136	1.702 ± 0.264
4–5	1.443 ± 0.124	1.403 ± 0.103	1.299 ± 0.101	1.475 ± 0.141	1.633 ± 0.260
5–6	1.601 ± 0.139	1.477 ± 0.109	1.539 ± 0.118	1.514 ± 0.148	1.896 ± 0.308
6–7	1.495 ± 0.135	1.524 ± 0.115	1.539 ± 0.119	1.676 ± 0.165	2.131 ± 0.351
7–8	1.618 ± 0.149	1.376 ± 0.108	1.643 ± 0.125	1.680 ± 0.160	2.198 ± 0.355
8–9	1.593 ± 0.152	1.438 ± 0.116	1.704 ± 0.132	1.565 ± 0.169	2.494 ± 0.447
9–10	1.724 ± 0.170	1.607 ± 0.130	1.689 ± 0.138	1.609 ± 0.176	2.538 ± 0.533
10–11	1.797 ± 0.199	1.431 ± 0.125	1.566 ± 0.136	1.645 ± 0.186	2.253 ± 0.474
11–12	1.755 ± 0.210	1.687 ± 0.143	1.808 ± 0.166	1.610 ± 0.196	2.930 ± 0.689
12–13	1.451 ± 0.184	1.639 ± 0.146	1.870 ± 0.172	1.933 ± 0.239	3.684 ± 0.985
13–14	1.177 ± 0.174	1.727 ± 0.158	1.852 ± 0.189	2.167 ± 0.291	3.385 ± 0.851
14–15	1.478 ± 0.218	1.580 ± 0.163	1.574 ± 0.175	2.100 ± 0.311	
15–16	1.680 ± 0.245	1.848 ± 0.199	1.980 ± 0.231	1.941 ± 0.328	
16–17	2.348 ± 0.337	1.587 ± 0.189	1.888 ± 0.232	2.167 ± 0.419	
17–18	1.809 ± 0.315	1.824 ± 0.227	1.827 ± 0.262	1.913 ± 0.377	4.640 ± 1.254
18–19	1.958 ± 0.319	2.109 ± 0.274	1.937 ± 0.304	1.977 ± 0.460	
19–20	1.987 ± 0.357	1.696 ± 0.244	2.075 ± 0.369	2.116 ± 0.536	
20–21	1.532 ± 0.254	1.846 ± 0.234	2.536 ± 0.348		
21–22				3.255 ± 0.582	
22–23	1.744 ± 0.346	2.294 ± 0.313	2.580 ± 0.412		
23–24					
24–25	2.257 ± 0.466	1.510 ± 0.285	2.408 ± 0.461		
25–26					
26–27					
27–28	1.700 ± 0.316	2.215 ± 0.459	2.339 ± 0.495		
28–29		2.629 ± 0.654			
29–30					

Table 7: The cross-section ratios between 13 TeV and 8 TeV in different bins of p_T and y for $\Upsilon(3S)$.

Acknowledgements

We thank Kuang-Ta Chao, Yu Feng, Yan-Qing Ma, Hua-Sheng Shao and Jian-Xiong Wang for frequent and interesting discussions on the production of Υ mesons. We express our gratitude to our colleagues in the CERN accelerator departments for the excellent performance of the LHC. We thank the technical and administrative staff at the LHCb institutes. We acknowledge support from CERN and from the national agencies: CAPES, CNPq, FAPERJ and FINEP (Brazil); MOST and NSFC (China); CNRS/IN2P3 (France); BMBF, DFG and MPG (Germany); INFN (Italy); NWO (The Netherlands); MNiSW and NCN (Poland); MEN/IFA (Romania); MinES and FASO (Russia); MinECo (Spain); SNSF and SER (Switzerland); NASU (Ukraine); STFC (United Kingdom); NSF (USA). We acknowledge the computing resources that are provided by CERN, IN2P3 (France), KIT and DESY (Germany), INFN (Italy), SURF (The Netherlands), PIC (Spain), GridPP (United Kingdom), RRCKI and Yandex LLC (Russia), CSCS (Switzerland), IFIN-HH (Romania), CBPF (Brazil), PL-GRID (Poland) and OSC (USA). We are indebted to the communities behind the multiple open-source software packages on which we depend. Individual groups or members have received support from AvH Foundation (Germany), EPLANET, Marie Skłodowska-Curie Actions and ERC (European Union), ANR, Labex P2IO and OCEVU, and Région Auvergne-Rhône-Alpes (France), Key Research Program of Frontier Sciences of CAS, CAS PIFI, and the Thousand Talents Program (China), RFBR, RSF and Yandex LLC (Russia), GVA, XuntaGal and GENCAT (Spain), Herchel Smith Fund, the Royal Society, the English-Speaking Union and the Leverhulme Trust (United Kingdom).

References

- [1] C. E. Carlson and R. Suaya, *Hadronic production of ψ/J meson*, Phys. Rev. **D14** (1976) 3115.
- [2] A. Donnachie and P. V. Landshoff, *Production of lepton pairs, J/ψ and charm with hadron beams*, Nucl. Phys. **B112** (1976) 233.
- [3] S. D. Ellis, M. B. Einhorn, and C. Quigg, *Comment on hadronic production of psions*, Phys. Rev. Lett. **36** (1976) 1263.
- [4] H. Fritzsch, *Producing heavy quark flavors in hadronic collisions: a test of quantum chromodynamics*, Phys. Lett. **B67** (1977) 217.
- [5] M. Gluck, J. F. Owens, and E. Reya, *Gluon contribution to hadronic J/ψ production*, Phys. Rev. **D17** (1978) 2324.
- [6] C.-H. Chang, *Hadronic production of J/ψ associated with a gluon*, Nucl. Phys. **B172** (1980) 425.
- [7] R. Baier and R. Rückl, *Hadronic production of J/ψ and Υ : transverse momentum distributions*, Phys. Lett. **B102** (1981) 364.
- [8] G. T. Bodwin, E. Braaten, and G. P. Lepage, *Rigorous QCD analysis of inclusive annihilation and production of heavy quarkonium*, Phys. Rev. **D51** (1995) 1125, arXiv:hep-ph/9407339, Erratum-ibid. **D55** (1997) 5853.

- [9] P. L. Cho and A. K. Leibovich, *Color-octet quarkonia production*, Phys. Rev. **D53** (1996) 150, [arXiv:hep-ph/9505329](#).
- [10] P. L. Cho and A. K. Leibovich, *Color-octet quarkonia production. II*, Phys. Rev. **D53** (1996) 6203, [arXiv:hep-ph/9511315](#).
- [11] ATLAS, G. Aad *et al.*, *Measurement of the $\Upsilon(1S)$ production cross-section in pp collisions at $\sqrt{s} = 7 \text{ TeV}$ in ATLAS*, Phys. Lett. **B705** (2011) 9, [arXiv:1106.5325](#).
- [12] ATLAS, G. Aad *et al.*, *Measurement of upsilon production in 7 TeV pp collisions at ATLAS*, Phys. Rev. **D87** (2013) 052004, [arXiv:1211.7255](#).
- [13] CMS collaboration, S. C. et al. *Measurement of the $\Upsilon(1S)$, $\Upsilon(2S)$ and $\Upsilon(3S)$ cross sections in pp collisions at $\sqrt{s} = 7 \text{ TeV}$* , Phys. Lett. **B727** (2013) 101, [arXiv:1303.5900](#).
- [14] CMS collaboration, S. C. et al. *Measurement of quarkonium production cross sections in pp collisions at $\sqrt{s} = 13 \text{ TeV}$* , Phys. Lett. **B780** (2018) 251, [arXiv:1710.11002](#).
- [15] LHCb collaboration, R. Aaij *et al.*, *Measurement of Υ production in pp collisions at $\sqrt{s} = 2.76 \text{ TeV}$* , Eur. Phys. J. **C74** (2014) 2835, [arXiv:1402.2539](#).
- [16] LHCb collaboration, R. Aaij *et al.*, *Measurement of Υ production in pp collisions at $\sqrt{s} = 7 \text{ TeV}$* , Eur. Phys. J. **C72** (2012) 2025, [arXiv:1202.6579](#).
- [17] LHCb collaboration, R. Aaij *et al.*, *Measurement of the exclusive Υ production cross-section in pp collisions at $\sqrt{s} = 7 \text{ TeV}$ and 8 TeV* , JHEP **09** (2015) 084, [arXiv:1505.08139](#).
- [18] LHCb collaboration, R. Aaij *et al.*, *Forward production of Υ mesons in pp collisions at $\sqrt{s} = 7$ and 8 TeV* , JHEP **11** (2015) 103, [arXiv:1509.02372](#).
- [19] LHCb collaboration, R. Aaij *et al.*, *Measurement of the $\Upsilon(nS)$ polarizations in pp collisions at $\sqrt{s} = 7$ and 8 TeV* , JHEP **12** (2017) 110, [arXiv:1709.01301](#).
- [20] LHCb collaboration, R. Aaij *et al.*, *Production of J/ψ and Υ mesons in pp collisions at $\sqrt{s} = 8 \text{ TeV}$* , JHEP **06** (2013) 064, [arXiv:1304.6977](#).
- [21] H. Han *et al.*, *$\Upsilon(nS)$ and $\chi_b(nP)$ production at hadron colliders in nonrelativistic QCD*, Phys. Rev. **D94** (2016) 014028, [arXiv:1410.8537](#).
- [22] L. S. Kisslinger and D. Das, *ψ and Υ production in pp collisions at 7.0 TeV*, Mod. Phys. Lett. **A28** (2013) 1350120, [arXiv:1306.6616](#).
- [23] L. S. Kisslinger and D. Das, *ψ and Υ production in pp collisions at 8.0 TeV*, Mod. Phys. Lett. **A29** (2014) 1450082, [arXiv:1403.2271](#).
- [24] Y. Feng, B. Gong, L.-P. Wan, and J.-X. Wang, *An updated study of Υ production and polarization at the Tevatron and LHC*, Chin. Phys. **C 39** (2015) 123102, [arXiv:1503.08439](#).
- [25] LHCb collaboration, A. A. Alves Jr. *et al.*, *The LHCb detector at the LHC*, JINST **3** (2008) S08005.

- [26] LHCb collaboration, R. Aaij *et al.*, *LHCb detector performance*, Int. J. Mod. Phys. **A30** (2015) 1530022, [arXiv:1412.6352](#).
- [27] R. Aaij *et al.*, *Performance of the LHCb Vertex Locator*, JINST **9** (2014) P09007, [arXiv:1405.7808](#).
- [28] R. Arink *et al.*, *Performance of the LHCb Outer Tracker*, JINST **9** (2014) P01002, [arXiv:1311.3893](#).
- [29] M. Adinolfi *et al.*, *Performance of the LHCb RICH detector at the LHC*, Eur. Phys. J. **C73** (2013) 2431, [arXiv:1211.6759](#).
- [30] A. A. Alves Jr. *et al.*, *Performance of the LHCb muon system*, JINST **8** (2013) P02022, [arXiv:1211.1346](#).
- [31] R. Aaij *et al.*, *The LHCb trigger and its performance in 2011*, JINST **8** (2013) P04022, [arXiv:1211.3055](#).
- [32] W. D. Hulsbergen, *Decay chain fitting with a Kalman filter*, Nucl. Instrum. Meth. **A552** (2005) 566, [arXiv:physics/0503191](#).
- [33] G. Dujany and B. Storaci, *Real-time alignment and calibration of the LHCb detector in Run II*, J. Phys. Conf. Ser. **664** (2015) 082010.
- [34] R. Aaij *et al.*, *Tesla: An application for real-time data analysis in High Energy Physics*, Comput. Phys. Commun. **208** (2016) 35, [arXiv:1604.05596](#).
- [35] T. Sjöstrand, S. Mrenna, and P. Skands, *A brief introduction to PYTHIA 8.1*, Comput. Phys. Commun. **178** (2008) 852, [arXiv:0710.3820](#).
- [36] I. Belyaev *et al.*, *Handling of the generation of primary events in Gauss, the LHCb simulation framework*, J. Phys. Conf. Ser. **331** (2011) 032047.
- [37] D. J. Lange, *The EvtGen particle decay simulation package*, Nucl. Instrum. Meth. **A462** (2001) 152.
- [38] P. Golonka and Z. Was, *PHOTOS Monte Carlo: A precision tool for QED corrections in Z and W decays*, Eur. Phys. J. **C45** (2006) 97, [arXiv:hep-ph/0506026](#).
- [39] Geant4 collaboration, J. Allison *et al.*, *Geant4 developments and applications*, IEEE Trans. Nucl. Sci. **53** (2006) 270.
- [40] T. Skwarnicki, *A study of the radiative cascade transitions between the Upsilon-prime and Upsilon resonances*, PhD thesis, Institute of Nuclear Physics, Krakow, 1986, DESY-F31-86-02.
- [41] Particle Data Group, C. Patrignani *et al.*, *Review of particle physics*, Chin. Phys. **C40** (2016) 100001.
- [42] LHCb collaboration, R. Aaij *et al.*, *Measurement of the track reconstruction efficiency at LHCb*, JINST **10** (2015) P02007, [arXiv:1408.1251](#).

- [43] LHCb collaboration, R. Aaij *et al.*, *Measurement of the b-quark production cross section in 7 and 13 TeV pp collisions*, Phys. Rev. Lett. **118** (2017) 052002, Erratum ibid. **119** (2017) 169901, [arXiv:1612.05140](https://arxiv.org/abs/1612.05140).
- [44] LHCb collaboration, R. Aaij *et al.*, *Precision luminosity measurements at LHCb*, JINST **9** (2014) P12005, [arXiv:1410.0149](https://arxiv.org/abs/1410.0149).
- [45] M. Jacob and G. C. Wick, *On the general theory of collisions for particles with spin*, Annals Phys. **7** (1959) 404.

LHCb collaboration

R. Aaij⁴³, B. Adeva³⁹, M. Adinolfi⁴⁸, Z. Ajaltouni⁵, S. Akar⁵⁹, J. Albrecht¹⁰, F. Alessio⁴⁰, M. Alexander⁵³, A. Alfonso Albero³⁸, S. Ali⁴³, G. Alkhazov³¹, P. Alvarez Cartelle⁵⁵, A.A. Alves Jr⁵⁹, S. Amato², S. Amerio²³, Y. Amhis⁷, L. An³, L. Anderlini¹⁸, G. Andreassi⁴¹, M. Andreotti^{17,g}, J.E. Andrews⁶⁰, R.B. Appleby⁵⁶, F. Archilli⁴³, P. d'Argent¹², J. Arnau Romeu⁶, A. Artamonov³⁷, M. Artuso⁶¹, E. Aslanides⁶, M. Atzeni⁴², G. Auriemma²⁶, S. Bachmann¹², J.J. Back⁵⁰, C. Baesso⁶², S. Baker⁵⁵, V. Balagura^{7,b}, W. Baldini¹⁷, A. Baranov³⁵, R.J. Barlow⁵⁶, S. Barsuk⁷, W. Barter⁵⁶, F. Baryshnikov³², V. Batozskaya²⁹, V. Battista⁴¹, A. Bay⁴¹, J. Beddow⁵³, F. Bedeschi²⁴, I. Bediaga¹, A. Beiter⁶¹, L.J. Bel⁴³, N. Belyi⁶³, V. Bellee⁴¹, N. Belloli^{21,i}, K. Belous³⁷, I. Belyaev^{32,40}, E. Ben-Haim⁸, G. Bencivenni¹⁹, S. Benson⁴³, S. Beranek⁹, A. Berezhnoy³³, R. Bernet⁴², D. Berninghoff¹², E. Bertholet⁸, A. Bertolin²³, C. Betancourt⁴², F. Betti^{15,40}, M.O. Bettler⁴⁹, M. van Beuzekom⁴³, Ia. Bezshyiko⁴², S. Bifani⁴⁷, P. Billoir⁸, A. Birnkraut¹⁰, A. Bizzeti^{18,u}, M. Bjørn⁵⁷, T. Blake⁵⁰, F. Blanc⁴¹, S. Blusk⁶¹, V. Bocci²⁶, T. Boettcher⁵⁸, A. Bondar^{36,w}, N. Bondar³¹, S. Borghi^{56,40}, M. Borisyak³⁵, M. Borsato³⁹, F. Bossu⁷, M. Boubdir⁹, T.J.V. Bowcock⁵⁴, E. Bowen⁴², C. Bozzi^{17,40}, S. Braun¹², M. Brodski⁴⁰, J. Brodzicka²⁷, D. Brundu¹⁶, E. Buchanan⁴⁸, C. Burr⁵⁶, A. Bursche¹⁶, J. Buytaert⁴⁰, W. Byczynski⁴⁰, S. Cadeddu¹⁶, H. Cai⁶⁴, R. Calabrese^{17,g}, R. Calladine⁴⁷, M. Calvi^{21,i}, M. Calvo Gomez^{38,m}, A. Camboni^{38,m}, P. Campana¹⁹, D.H. Campora Perez⁴⁰, L. Capriotti⁵⁶, A. Carbone^{15,e}, G. Carboni²⁵, R. Cardinale^{20,h}, A. Cardini¹⁶, P. Carniti^{21,i}, L. Carson⁵², K. Carvalho Akiba², G. Casse⁵⁴, L. Cassina²¹, M. Cattaneo⁴⁰, G. Cavallero^{20,h}, R. Cenci^{24,t}, D. Chamont⁷, M.G. Chapman⁴⁸, M. Charles⁸, Ph. Charpentier⁴⁰, G. Chatzikonstantinidis⁴⁷, M. Chefdeville⁴, S. Chen¹⁶, S.-G. Chitic⁴⁰, V. Chobanova³⁹, M. Chrzaszcz⁴⁰, A. Chubykin³¹, P. Ciambrone¹⁹, X. Cid Vidal³⁹, G. Ciezarek⁴⁰, P.E.L. Clarke⁵², M. Clemencic⁴⁰, H.V. Cliff⁴⁹, J. Closier⁴⁰, V. Coco⁴⁰, J. Cogan⁶, E. Cogneras⁵, V. Cogoni^{16,f}, L. Cojocariu³⁰, P. Collins⁴⁰, T. Colombo⁴⁰, A. Comerma-Montells¹², A. Contu¹⁶, G. Coombs⁴⁰, S. Coquereau³⁸, G. Corti⁴⁰, M. Corvo^{17,g}, C.M. Costa Sobral⁵⁰, B. Couturier⁴⁰, G.A. Cowan⁵², D.C. Craik⁵⁸, A. Crocombe⁵⁰, M. Cruz Torres¹, R. Currie⁵², C. D'Ambrosio⁴⁰, F. Da Cunha Marinho², C.L. Da Silva⁷³, E. Dall'Occo⁴³, J. Dalseno⁴⁸, A. Davis³, O. De Aguiar Francisco⁴⁰, K. De Bruyn⁴⁰, S. De Capua⁵⁶, M. De Cian¹², J.M. De Miranda¹, L. De Paula², M. De Serio^{14,d}, P. De Simone¹⁹, C.T. Dean⁵³, D. Decamp⁴, L. Del Buono⁸, B. Delaney⁴⁹, H.-P. Dembinski¹¹, M. Demmer¹⁰, A. Dendek²⁸, D. Derkach³⁵, O. Deschamps⁵, F. Dettori⁵⁴, B. Dey⁶⁵, A. Di Canto⁴⁰, P. Di Nezza¹⁹, S. Didenko⁶⁹, H. Dijkstra⁴⁰, F. Dordei⁴⁰, M. Dorigo⁴⁰, A. Dosil Suárez³⁹, L. Douglas⁵³, A. Dovbnya⁴⁵, K. Dreimanis⁵⁴, L. Dufour⁴³, G. Dujany⁸, P. Durante⁴⁰, J.M. Durham⁷³, D. Dutta⁵⁶, R. Dzhelyadin³⁷, M. Dziewiecki¹², A. Dziurda⁴⁰, A. Dzyuba³¹, S. Easo⁵¹, U. Egede⁵⁵, V. Egorychev³², S. Eidelman^{36,w}, S. Eisenhardt⁵², U. Eitschberger¹⁰, R. Ekelhof¹⁰, L. Eklund⁵³, S. Ely⁶¹, A. Ene³⁰, S. Escher⁹, S. Esen¹², H.M. Evans⁴⁹, T. Evans⁵⁷, A. Falabella¹⁵, N. Farley⁴⁷, S. Farry⁵⁴, D. Fazzini^{21,40,i}, L. Federici²⁵, G. Fernandez³⁸, P. Fernandez Declara⁴⁰, A. Fernandez Prieto³⁹, F. Ferrari¹⁵, L. Ferreira Lopes⁴¹, F. Ferreira Rodrigues², M. Ferro-Luzzi⁴⁰, S. Filippov³⁴, R.A. Fini¹⁴, M. Fiorini^{17,g}, M. Firlej²⁸, C. Fitzpatrick⁴¹, T. Fiutowski²⁸, F. Fleuret^{7,b}, M. Fontana^{16,40}, F. Fontanelli^{20,h}, R. Forty⁴⁰, V. Franco Lima⁵⁴, M. Frank⁴⁰, C. Frei⁴⁰, J. Fu^{22,q}, W. Funk⁴⁰, C. Färber⁴⁰, E. Gabriel⁵², A. Gallas Torreira³⁹, D. Galli^{15,e}, S. Gallorini²³, S. Gambetta⁵², M. Gandelman², P. Gandini²², Y. Gao³, L.M. Garcia Martin⁷¹, J. García Pardiñas³⁹, J. Garra Tico⁴⁹, L. Garrido³⁸, D. Gascon³⁸, C. Gaspar⁴⁰, L. Gavardi¹⁰, G. Gazzoni⁵, D. Gerick¹², E. Gersabeck⁵⁶, M. Gersabeck⁵⁶, T. Gershon⁵⁰, Ph. Ghez⁴, S. Giani⁴¹, V. Gibson⁴⁹, O.G. Girard⁴¹, L. Giubega³⁰, K. Gizdov⁵², V.V. Gligorov⁸, D. Golubkov³², A. Golutvin^{55,69}, A. Gomes^{1,a}, I.V. Gorelov³³, C. Gotti^{21,i}, E. Govorkova⁴³, J.P. Grabowski¹², R. Graciani Diaz³⁸, L.A. Granado Cardoso⁴⁰, E. Graugés³⁸, E. Graverini⁴², G. Graziani¹⁸, A. Grecu³⁰, R. Greim⁴³, P. Griffith¹⁶, L. Grillo⁵⁶, L. Gruber⁴⁰, B.R. Gruberg Cazon⁵⁷, O. Grünberg⁶⁷, E. Gushchin³⁴,

Yu. Guz³⁷, T. Gys⁴⁰, C. Göbel⁶², T. Hadavizadeh⁵⁷, C. Hadjivasiliou⁵, G. Haefeli⁴¹, C. Haen⁴⁰, S.C. Haines⁴⁹, B. Hamilton⁶⁰, X. Han¹², T.H. Hancock⁵⁷, S. Hansmann-Menzemer¹², N. Harnew⁵⁷, S.T. Harnew⁴⁸, C. Hasse⁴⁰, M. Hatch⁴⁰, J. He⁶³, M. Hecker⁵⁵, K. Heinicke¹⁰, A. Heister⁹, K. Hennessy⁵⁴, L. Henry⁷¹, E. van Herwijnen⁴⁰, M. Heß⁶⁷, A. Hicheur², D. Hill⁵⁷, P.H. Hopchev⁴¹, W. Hu⁶⁵, W. Huang⁶³, Z.C. Huard⁵⁹, W. Hulsbergen⁴³, T. Humair⁵⁵, M. Hushchyn³⁵, D. Hutchcroft⁵⁴, P. Ibis¹⁰, M. Idzik²⁸, P. Ilten⁴⁷, R. Jacobsson⁴⁰, J. Jalocha⁵⁷, E. Jans⁴³, A. Jawahery⁶⁰, F. Jiang³, M. John⁵⁷, D. Johnson⁴⁰, C.R. Jones⁴⁹, C. Joram⁴⁰, B. Jost⁴⁰, N. Jurik⁵⁷, S. Kandybei⁴⁵, M. Karacson⁴⁰, J.M. Kariuki⁴⁸, S. Karodia⁵³, N. Kazeev³⁵, M. Kecke¹², F. Keizer⁴⁹, M. Kelsey⁶¹, M. Kenzie⁴⁹, T. Ketel⁴⁴, E. Khairullin³⁵, B. Khanji¹², C. Khurewathanakul⁴¹, K.E. Kim⁶¹, T. Kirn⁹, S. Klaver¹⁹, K. Klimaszewski²⁹, T. Klimkovich¹¹, S. Koliiev⁴⁶, M. Kolpin¹², R. Kopecna¹², P. Koppenburg⁴³, S. Kotriakhova³¹, M. Kozeiha⁵, L. Kravchuk³⁴, M. Kreps⁵⁰, F. Kress⁵⁵, P. Krokovny^{36,w}, W. Krupa²⁸, W. Krzemien²⁹, W. Kucewicz^{27,l}, M. Kucharczyk²⁷, V. Kudryavtsev^{36,w}, A.K. Kuonen⁴¹, T. Kvaratskheliya^{32,40}, D. Lacarrere⁴⁰, G. Lafferty⁵⁶, A. Lai¹⁶, G. Lanfranchi¹⁹, C. Langenbruch⁹, T. Latham⁵⁰, C. Lazzeroni⁴⁷, R. Le Gac⁶, A. Leflat^{33,40}, J. Lefrançois⁷, R. Lefèvre⁵, F. Lemaitre⁴⁰, O. Leroy⁶, T. Lesiak²⁷, B. Leverington¹², P.-R. Li⁶³, T. Li³, Y. Li⁷, Z. Li⁶¹, X. Liang⁶¹, T. Likhomanenko⁶⁸, R. Lindner⁴⁰, F. Lionetto⁴², V. Lisovskyi⁷, X. Liu³, D. Loh⁵⁰, A. Loi¹⁶, I. Longstaff⁵³, J.H. Lopes², D. Lucchesi^{23,o}, M. Lucio Martinez³⁹, A. Lupato²³, E. Luppi^{17,g}, O. Lupton⁴⁰, A. Lusiani²⁴, X. Lyu⁶³, F. Machefert⁷, F. Maciuc³⁰, V. Macko⁴¹, P. Mackowiak¹⁰, S. Maddrell-Mander⁴⁸, O. Maev^{31,40}, K. Maguire⁵⁶, D. Maisuzenko³¹, M.W. Majewski²⁸, S. Malde⁵⁷, B. Malecki²⁷, A. Malinin⁶⁸, T. Maltsev^{36,w}, G. Manca^{16,f}, G. Mancinelli⁶, D. Marangotto^{22,q}, J. Maratas^{5,v}, J.F. Marchand⁴, U. Marconi¹⁵, C. Marin Benito³⁸, M. Marinangeli⁴¹, P. Marino⁴¹, J. Marks¹², G. Martellotti²⁶, M. Martin⁶, M. Martinelli⁴¹, D. Martinez Santos³⁹, F. Martinez Vidal⁷¹, A. Massafferri¹, R. Matev⁴⁰, A. Mathad⁵⁰, Z. Mathe⁴⁰, C. Matteuzzi²¹, A. Mauri⁴², E. Maurice^{7,b}, B. Maurin⁴¹, A. Mazurov⁴⁷, M. McCann^{55,40}, A. McNab⁵⁶, R. McNulty¹³, J.V. Mead⁵⁴, B. Meadows⁵⁹, C. Meaux⁶, F. Meier¹⁰, N. Meinert⁶⁷, D. Melnychuk²⁹, M. Merk⁴³, A. Merli^{22,q}, E. Michielin²³, D.A. Milanes⁶⁶, E. Millard⁵⁰, M.-N. Minard⁴, L. Minzoni^{17,g}, D.S. Mitzel¹², A. Mogini⁸, J. Molina Rodriguez^{1,y}, T. Mombächer¹⁰, I.A. Monroy⁶⁶, S. Monteil⁵, M. Morandin²³, G. Morello¹⁹, M.J. Morello^{24,t}, O. Morgunova⁶⁸, J. Moron²⁸, A.B. Morris⁶, R. Mountain⁶¹, F. Muheim⁵², M. Mulder⁴³, D. Müller⁴⁰, J. Müller¹⁰, K. Müller⁴², V. Müller¹⁰, P. Naik⁴⁸, T. Nakada⁴¹, R. Nandakumar⁵¹, A. Nandi⁵⁷, I. Nasteva², M. Needham⁵², N. Neri²², S. Neubert¹², N. Neufeld⁴⁰, M. Neuner¹², T.D. Nguyen⁴¹, C. Nguyen-Mau^{41,n}, S. Nieswand⁹, R. Niet¹⁰, N. Nikitin³³, A. Nogay⁶⁸, D.P. O'Hanlon¹⁵, A. Oblakowska-Mucha²⁸, V. Obraztsov³⁷, S. Ogilvy¹⁹, R. Oldeman^{16,f}, C.J.G. Onderwater⁷², A. Ossowska²⁷, J.M. Otalora Goicochea², P. Owen⁴², A. Oyanguren⁷¹, P.R. Pais⁴¹, A. Palano¹⁴, M. Palutan^{19,40}, G. Panshin⁷⁰, A. Papanestis⁵¹, M. Pappagallo⁵², L.L. Pappalardo^{17,g}, W. Parker⁶⁰, C. Parkes⁵⁶, G. Passaleva^{18,40}, A. Pastore¹⁴, M. Patel⁵⁵, C. Patrignani^{15,e}, A. Pearce⁴⁰, A. Pellegrino⁴³, G. Penso²⁶, M. Pepe Altarelli⁴⁰, S. Perazzini⁴⁰, D. Pereima³², P. Perret⁵, L. Pescatore⁴¹, K. Petridis⁴⁸, A. Petrolini^{20,h}, A. Petrov⁶⁸, M. Petruzzo^{22,q}, B. Pietrzyk⁴, G. Pietrzyk⁴¹, M. Pikies²⁷, D. Pinci²⁶, F. Pisani⁴⁰, A. Pistone^{20,h}, A. Piucci¹², V. Placinta³⁰, S. Playfer⁵², M. Plo Casasus³⁹, F. Polci⁸, M. Poli Lener¹⁹, A. Poluektov⁵⁰, N. Polukhina⁶⁹, I. Polyakov⁶¹, E. Polycarpo², G.J. Pomery⁴⁸, S. Ponce⁴⁰, A. Popov³⁷, D. Popov^{11,40}, S. Poslavskii³⁷, C. Potterat², E. Price⁴⁸, J. Prisciandaro³⁹, C. Prouve⁴⁸, V. Pugatch⁴⁶, A. Puig Navarro⁴², H. Pullen⁵⁷, G. Punzi^{24,p}, W. Qian⁶³, J. Qin⁶³, R. Quagliani⁸, B. Quintana⁵, B. Rachwal²⁸, J.H. Rademacker⁴⁸, M. Rama²⁴, M. Ramos Pernas³⁹, M.S. Rangel², I. Raniuk^{45,†}, F. Ratnikov^{35,x}, G. Raven⁴⁴, M. Ravonel Salzgeber⁴⁰, M. Reboud⁴, F. Redi⁴¹, S. Reichert¹⁰, A.C. dos Reis¹, C. Remon Alepuz⁷¹, V. Renaudin⁷, S. Ricciardi⁵¹, S. Richards⁴⁸, K. Rinnert⁵⁴, P. Robbe⁷, A. Robert⁸, A.B. Rodrigues⁴¹, E. Rodrigues⁵⁹, J.A. Rodriguez Lopez⁶⁶, A. Rogozhnikov³⁵, S. Roiser⁴⁰, A. Rollings⁵⁷, V. Romanovskiy³⁷, A. Romero Vidal^{39,40},

M. Rotondo¹⁹, M.S. Rudolph⁶¹, T. Ruf⁴⁰, J. Ruiz Vidal⁷¹, J.J. Saborido Silva³⁹, N. Sagidova³¹, B. Saitta^{16,f}, V. Salustino Guimaraes⁶², C. Sanchez Mayordomo⁷¹, B. Sanmartin Sedes³⁹, R. Santacesaria²⁶, C. Santamarina Rios³⁹, M. Santimaria¹⁹, E. Santovetti^{25,j}, G. Sarpis⁵⁶, A. Sarti^{19,k}, C. Satriano^{26,s}, A. Satta²⁵, D.M. Saunders⁴⁸, D. Savrina^{32,33}, S. Schael⁹, M. Schellenberg¹⁰, M. Schiller⁵³, H. Schindler⁴⁰, M. Schmelling¹¹, T. Schmelzer¹⁰, B. Schmidt⁴⁰, O. Schneider⁴¹, A. Schopper⁴⁰, H.F. Schreiner⁵⁹, M. Schubiger⁴¹, M.H. Schune^{7,40}, R. Schwemmer⁴⁰, B. Sciascia¹⁹, A. Sciubba^{26,k}, A. Semennikov³², E.S. Sepulveda⁸, A. Sergi⁴⁷, N. Serra⁴², J. Serrano⁶, L. Sestini²³, P. Seyfert⁴⁰, M. Shapkin³⁷, Y. Shcheglov^{31,†}, T. Shears⁵⁴, L. Shekhtman^{36,w}, V. Shevchenko⁶⁸, B.G. Siddi¹⁷, R. Silva Coutinho⁴², L. Silva de Oliveira², G. Simi^{23,o}, S. Simone^{14,d}, N. Skidmore¹², T. Skwarnicki⁶¹, I.T. Smith⁵², M. Smith⁵⁵, I. Soares Lavra¹, M.D. Sokoloff⁵⁹, F.J.P. Soler⁵³, B. Souza De Paula², B. Spaan¹⁰, P. Spradlin⁵³, F. Stagni⁴⁰, M. Stahl¹², S. Stahl⁴⁰, P. Steffko⁴¹, S. Stefkova⁵⁵, O. Steinkamp⁴², S. Stemmle¹², O. Stenyakin³⁷, M. Stepanova³¹, H. Stevens¹⁰, S. Stone⁶¹, B. Storaci⁴², S. Stracka^{24,p}, M.E. Stramaglia⁴¹, M. Straticiuc³⁰, U. Straumann⁴², S. Strokov⁷⁰, J. Sun³, L. Sun⁶⁴, K. Swientek²⁸, V. Syropoulos⁴⁴, T. Szumlak²⁸, M. Szymanski⁶³, S. T'Jampens⁴, Z. Tang³, A. Tayduganov⁶, T. Tekampe¹⁰, G. Tellarini¹⁷, F. Teubert⁴⁰, E. Thomas⁴⁰, J. van Tilburg⁴³, M.J. Tilley⁵⁵, V. Tisserand⁵, M. Tobin⁴¹, S. Tolk⁴⁰, L. Tomassetti^{17,g}, D. Tonelli²⁴, R. Tourinho Jadallah Aoude¹, E. Tournefier⁴, M. Traill⁵³, M.T. Tran⁴¹, M. Tresch⁴², A. Trisovic⁴⁹, A. Tsaregorodtsev⁶, A. Tully⁴⁹, N. Tuning^{43,40}, A. Ukleja²⁹, A. Usachov⁷, A. Ustyuzhanin³⁵, U. Uwer¹², C. Vacca^{16,f}, A. Vagner⁷⁰, V. Vagnoni¹⁵, A. Valassi⁴⁰, S. Valat⁴⁰, G. Valenti¹⁵, R. Vazquez Gomez⁴⁰, P. Vazquez Regueiro³⁹, S. Vecchi¹⁷, M. van Veghel⁴³, J.J. Velthuis⁴⁸, M. Veltri^{18,r}, G. Veneziano⁵⁷, A. Venkateswaran⁶¹, T.A. Verlage⁹, M. Vernet⁵, M. Vesterinen⁵⁷, J.V. Viana Barbosa⁴⁰, D. Vieira⁶³, M. Vieites Diaz³⁹, H. Viemann⁶⁷, X. Vilasis-Cardona^{38,m}, A. Vitkovskiy⁴³, M. Vitti⁴⁹, V. Volkov³³, A. Vollhardt⁴², B. Voneki⁴⁰, A. Vorobyev³¹, V. Vorobyev^{36,w}, C. Voß⁹, J.A. de Vries⁴³, C. Vázquez Sierra⁴³, R. Waldi⁶⁷, J. Walsh²⁴, J. Wang⁶¹, M. Wang³, Y. Wang⁶⁵, D.R. Ward⁴⁹, H.M. Wark⁵⁴, N.K. Watson⁴⁷, D. Websdale⁵⁵, A. Weiden⁴², C. Weisser⁵⁸, M. Whitehead⁹, J. Wicht⁵⁰, G. Wilkinson⁵⁷, M. Wilkinson⁶¹, M.R.J. Williams⁵⁶, M. Williams⁵⁸, T. Williams⁴⁷, F.F. Wilson^{51,40}, J. Wimberley⁶⁰, M. Winn⁷, J. Wishahi¹⁰, W. Wislicki²⁹, M. Witek²⁷, G. Wormser⁷, S.A. Wotton⁴⁹, K. Wyllie⁴⁰, Y. Xie⁶⁵, M. Xu⁶⁵, Q. Xu⁶³, Z. Xu³, Z. Xu⁴, Z. Yang³, Z. Yang⁶⁰, Y. Yao⁶¹, H. Yin⁶⁵, J. Yu⁶⁵, X. Yuan⁶¹, O. Yushchenko³⁷, K.A. Zarebski⁴⁷, M. Zavertyaev^{11,c}, L. Zhang³, Y. Zhang⁷, A. Zhelezov¹², Y. Zheng⁶³, X. Zhu³, V. Zhukov^{9,33}, J.B. Zonneveld⁵², S. Zucchelli¹⁵.

¹Centro Brasileiro de Pesquisas Físicas (CBPF), Rio de Janeiro, Brazil

²Universidade Federal do Rio de Janeiro (UFRJ), Rio de Janeiro, Brazil

³Center for High Energy Physics, Tsinghua University, Beijing, China

⁴Univ. Grenoble Alpes, Univ. Savoie Mont Blanc, CNRS, IN2P3-LAPP, Annecy, France

⁵Clermont Université, Université Blaise Pascal, CNRS/IN2P3, LPC, Clermont-Ferrand, France

⁶Aix Marseille Univ, CNRS/IN2P3, CPPM, Marseille, France

⁷LAL, Univ. Paris-Sud, CNRS/IN2P3, Université Paris-Saclay, Orsay, France

⁸LPNHE, Université Pierre et Marie Curie, Université Paris Diderot, CNRS/IN2P3, Paris, France

⁹I. Physikalisches Institut, RWTH Aachen University, Aachen, Germany

¹⁰Fakultät Physik, Technische Universität Dortmund, Dortmund, Germany

¹¹Max-Planck-Institut für Kernphysik (MPIK), Heidelberg, Germany

¹²Physikalischs Institut, Ruprecht-Karls-Universität Heidelberg, Heidelberg, Germany

¹³School of Physics, University College Dublin, Dublin, Ireland

¹⁴Sezione INFN di Bari, Bari, Italy

¹⁵Sezione INFN di Bologna, Bologna, Italy

¹⁶Sezione INFN di Cagliari, Cagliari, Italy

¹⁷Sezione INFN di Ferrara, Ferrara, Italy

¹⁸Sezione INFN di Firenze, Firenze, Italy

- ¹⁹*Laboratori Nazionali dell'INFN di Frascati, Frascati, Italy*
- ²⁰*Sezione INFN di Genova, Genova, Italy*
- ²¹*Sezione INFN di Milano Bicocca, Milano, Italy*
- ²²*Sezione INFN di Milano, Milano, Italy*
- ²³*Sezione INFN di Padova, Padova, Italy*
- ²⁴*Sezione INFN di Pisa, Pisa, Italy*
- ²⁵*Sezione INFN di Roma Tor Vergata, Roma, Italy*
- ²⁶*Sezione INFN di Roma La Sapienza, Roma, Italy*
- ²⁷*Henryk Niewodniczanski Institute of Nuclear Physics Polish Academy of Sciences, Kraków, Poland*
- ²⁸*AGH - University of Science and Technology, Faculty of Physics and Applied Computer Science, Kraków, Poland*
- ²⁹*National Center for Nuclear Research (NCBJ), Warsaw, Poland*
- ³⁰*Horia Hulubei National Institute of Physics and Nuclear Engineering, Bucharest-Magurele, Romania*
- ³¹*Petersburg Nuclear Physics Institute (PNPI), Gatchina, Russia*
- ³²*Institute of Theoretical and Experimental Physics (ITEP), Moscow, Russia*
- ³³*Institute of Nuclear Physics, Moscow State University (SINP MSU), Moscow, Russia*
- ³⁴*Institute for Nuclear Research of the Russian Academy of Sciences (INR RAS), Moscow, Russia*
- ³⁵*Yandex School of Data Analysis, Moscow, Russia*
- ³⁶*Budker Institute of Nuclear Physics (SB RAS), Novosibirsk, Russia*
- ³⁷*Institute for High Energy Physics (IHEP), Protvino, Russia*
- ³⁸*ICCUB, Universitat de Barcelona, Barcelona, Spain*
- ³⁹*Instituto Galego de Física de Altas Enerxías (IGFAE), Universidade de Santiago de Compostela, Santiago de Compostela, Spain*
- ⁴⁰*European Organization for Nuclear Research (CERN), Geneva, Switzerland*
- ⁴¹*Institute of Physics, Ecole Polytechnique Fédérale de Lausanne (EPFL), Lausanne, Switzerland*
- ⁴²*Physik-Institut, Universität Zürich, Zürich, Switzerland*
- ⁴³*Nikhef National Institute for Subatomic Physics, Amsterdam, The Netherlands*
- ⁴⁴*Nikhef National Institute for Subatomic Physics and VU University Amsterdam, Amsterdam, The Netherlands*
- ⁴⁵*NSC Kharkiv Institute of Physics and Technology (NSC KIPT), Kharkiv, Ukraine*
- ⁴⁶*Institute for Nuclear Research of the National Academy of Sciences (KINR), Kyiv, Ukraine*
- ⁴⁷*University of Birmingham, Birmingham, United Kingdom*
- ⁴⁸*H.H. Wills Physics Laboratory, University of Bristol, Bristol, United Kingdom*
- ⁴⁹*Cavendish Laboratory, University of Cambridge, Cambridge, United Kingdom*
- ⁵⁰*Department of Physics, University of Warwick, Coventry, United Kingdom*
- ⁵¹*STFC Rutherford Appleton Laboratory, Didcot, United Kingdom*
- ⁵²*School of Physics and Astronomy, University of Edinburgh, Edinburgh, United Kingdom*
- ⁵³*School of Physics and Astronomy, University of Glasgow, Glasgow, United Kingdom*
- ⁵⁴*Oliver Lodge Laboratory, University of Liverpool, Liverpool, United Kingdom*
- ⁵⁵*Imperial College London, London, United Kingdom*
- ⁵⁶*School of Physics and Astronomy, University of Manchester, Manchester, United Kingdom*
- ⁵⁷*Department of Physics, University of Oxford, Oxford, United Kingdom*
- ⁵⁸*Massachusetts Institute of Technology, Cambridge, MA, United States*
- ⁵⁹*University of Cincinnati, Cincinnati, OH, United States*
- ⁶⁰*University of Maryland, College Park, MD, United States*
- ⁶¹*Syracuse University, Syracuse, NY, United States*
- ⁶²*Pontifícia Universidade Católica do Rio de Janeiro (PUC-Rio), Rio de Janeiro, Brazil, associated to ²*
- ⁶³*University of Chinese Academy of Sciences, Beijing, China, associated to ³*
- ⁶⁴*School of Physics and Technology, Wuhan University, Wuhan, China, associated to ³*
- ⁶⁵*Institute of Particle Physics, Central China Normal University, Wuhan, Hubei, China, associated to ³*
- ⁶⁶*Departamento de Fisica , Universidad Nacional de Colombia, Bogota, Colombia, associated to ⁸*
- ⁶⁷*Institut für Physik, Universität Rostock, Rostock, Germany, associated to ¹²*
- ⁶⁸*National Research Centre Kurchatov Institute, Moscow, Russia, associated to ³²*
- ⁶⁹*National University of Science and Technology MISIS, Moscow, Russia, associated to ³²*
- ⁷⁰*National Research Tomsk Polytechnic University, Tomsk, Russia, associated to ³²*
- ⁷¹*Instituto de Fisica Corpuscular, Centro Mixto Universidad de Valencia - CSIC, Valencia, Spain,*

*associated to*³⁸

⁷²*Van Swinderen Institute, University of Groningen, Groningen, The Netherlands, associated to*⁴³

⁷³*Los Alamos National Laboratory (LANL), Los Alamos, United States, associated to*⁶¹

^a*Universidade Federal do Triângulo Mineiro (UFTM), Uberaba-MG, Brazil*

^b*Laboratoire Leprince-Ringuet, Palaiseau, France*

^c*P.N. Lebedev Physical Institute, Russian Academy of Science (LPI RAS), Moscow, Russia*

^d*Università di Bari, Bari, Italy*

^e*Università di Bologna, Bologna, Italy*

^f*Università di Cagliari, Cagliari, Italy*

^g*Università di Ferrara, Ferrara, Italy*

^h*Università di Genova, Genova, Italy*

ⁱ*Università di Milano Bicocca, Milano, Italy*

^j*Università di Roma Tor Vergata, Roma, Italy*

^k*Università di Roma La Sapienza, Roma, Italy*

^l*AGH - University of Science and Technology, Faculty of Computer Science, Electronics and Telecommunications, Kraków, Poland*

^m*LIFAELS, La Salle, Universitat Ramon Llull, Barcelona, Spain*

ⁿ*Hanoi University of Science, Hanoi, Vietnam*

^o*Università di Padova, Padova, Italy*

^p*Università di Pisa, Pisa, Italy*

^q*Università degli Studi di Milano, Milano, Italy*

^r*Università di Urbino, Urbino, Italy*

^s*Università della Basilicata, Potenza, Italy*

^t*Scuola Normale Superiore, Pisa, Italy*

^u*Università di Modena e Reggio Emilia, Modena, Italy*

^v*MSU - Iligan Institute of Technology (MSU-IIT), Iligan, Philippines*

^w*Novosibirsk State University, Novosibirsk, Russia*

^x*National Research University Higher School of Economics, Moscow, Russia*

^y*Escuela Agrícola Panamericana, San Antonio de Oriente, Honduras*

[†]*Deceased*